NASA TR R-82

NATIONAL AERONAUTICS AND SPACE ADMINISTRATION

TECHNICAL REPORT

R-82

TURBULENT SKIN FRICTION AT HIGH MACH NUMBERS AND REYNOLDS NUMBERS IN AIR AND HELIUM

By FRED W. MATTING, DEAN R. CHAPMAN, JACK R. NYHOLM
and ANDREW G. THOMAS

1961

For sale by the Superintendent of Documents, U.S. Government Printing Office, Washington 25, D.C. Yearly subscription, $15; foreign, $19; single copy price varies according to size - - - - - - - - - Price 45 cents

TECHNICAL REPORT R-82

TURBULENT SKIN FRICTION AT HIGH MACH NUMBERS AND REYNOLDS NUMBERS IN AIR AND HELIUM

By FRED W. MATTING, DEAN R. CHAPMAN, JACK R. NYHOLM, and ANDREW G. THOMAS

Ames Research Center
Moffett Field, Calif.

TECHNICAL REPORT R–82

TURBULENT SKIN FRICTION AT HIGH MACH NUMBERS AND REYNOLDS NUMBERS IN AIR AND HELIUM

By Fred W. Matting, Dean R. Chapman, Jack R. Nyholm, and Andrew G. Thomas

SUMMARY

Mach number (i.e., incompressible) flow. The

I. Matting, Fred W.
II. Chapman, Dean R.
III. Nyholm, Jack R.
IV. Thomas, Andrew G.
V. NASA TR R-82

NASA

NASA TR R-82
National Aeronautics and Space Administration.
TURBULENT SKIN FRICTION AT HIGH MACH NUMBERS AND REYNOLDS NUMBERS IN AIR AND HELIUM. Fred W. Matting, Dean R. Chapman, Jack R. Nyholm, and Andrew G. Thomas. 1961. i, 39 p. diagrs., photo. GPO price 45 cents. (NASA TECHNICAL REPORT R-82)

Results are given of local skin-friction measurements in turbulent boundary layers over an equivalent air Mach number range from 0.2 to 9.9 and an over-all Reynolds number variation of 2×10^6 to 100×10^6. Direct force measurements were made by means of a floating element. Flows were two-dimensional over a smooth flat surface with essentially zero pressure gradient and with adiabatic conditions at the wall. Air and helium were used as working fluids. An equivalence parameter for comparing boundary layers in different working fluids is derived and the experimental verification of the parameter is demonstrated. Experimental results are compared with the results obtained by several methods of calculating skin friction in the turbulent boundary layer.
(Initial NASA distribution: 1, Aerodynamics, aircraft; 2, Aerodynamics, missiles and space vehicles; 20, Fluid mechanics; 37, Propulsion system elements.)

Copies obtainable from Supt. of Docs., GPO, Washington

I. Matting, Fred W.
II. Chapman, Dean R.
III. Nyholm, Jack R.
IV. Thomas, Andrew G.
V. NASA TR R-82

NASA

The program included the construction of a special apparatus, a 1- by 10-inch boundary-layer channel, with provisions for using both air and helium as test media. In connection with using helium, it was necessary to determine the equivalence of air and helium in the turbulent boundary layer. This is covered in some detail in later sections.

SYMBOLS

A area

a speed of sound

C_f coefficient of local skin friction, $\frac{\tau_w}{(1/2)\rho_\infty U_\infty^2}$

C_{f_i} coefficient of local skin friction for incompressible flow

C_p pressure coefficient, $\frac{p-p_\infty}{q_\infty}$

c_p specific heat at constant pressure

c_v specific heat at constant volume

h enthalpy per unit mass

k coefficient of thermal conductivity

L length from nozzle throat to center of skin-friction element

l characteristic reference length

M Mach number

M_a equivalent air Mach number (see eq. (9))

p static pressure

Pr Prandtl number, $\frac{c_p\mu}{k}$

Pr_{turb} turbulent Prandtl number, $\frac{c_p\epsilon}{\lambda}$

Q convective heat-transfer rate per unit area in the boundary layer in the y direction

Q_{turb} turbulent heat-transfer rate per unit area in the y direction

q_∞ dynamic pressure, $\frac{\gamma p_\infty M_\infty^2}{2}$, or $(1/2)\rho_\infty U_\infty^2$

R gas constant

Re_L Reynolds number based on L, $\frac{U_\infty\rho_\infty L}{\mu_\infty}$

Re_l Reynolds number based on l, $\frac{U_\infty\rho_\infty l}{\mu_\infty}$

Re_x Reynolds number at skin-friction element measured from transition point, $\frac{U_\infty\rho_\infty(L-x_{tr})}{\mu_\infty}=\frac{U_\infty\rho_\infty x}{\mu_\infty}$

Re_w Reynolds number based on wall properties, $\frac{U_\infty\rho_w l}{\mu_w}\left(\text{or } \frac{U_\infty\rho_w x}{\mu_w} \text{ when } x=l\right)$

T static temperature, °R

t static temperature, °F

u,v velocity components in the x and y directions, respectively

u_τ friction velocity, $\sqrt{\frac{\tau_w}{\rho_w}}$

u^* dimensionless velocity, $\frac{u}{u_\tau}$

U_∞ free-stream velocity

x coordinate parallel to free-stream flow direction and length from transition point to center of skin-friction element

x_{tr} length from nozzle throat to transition point

y coordinate perpendicular to the wall

y^* dimensionless y coordinate, $\frac{yu_\tau}{\nu_w}$

γ ratio of specific heats, $\frac{c_p}{c_v}$

Δ increment of a quantity (e.g., ΔM)

δ boundary-layer thickness

ϵ eddy viscosity, $\frac{\tau_{turb}}{\partial u/\partial y}$

η dimensionless coordinate perpendicular to the wall, $\frac{y}{l}$

η_r recovery factor, $\frac{T_{aw}-T_\infty}{T_t-T_\infty}$

θ boundary-layer momentum thickness, $\int_0^\delta \frac{\rho u}{\rho_\infty U_\infty}\left(1-\frac{u}{U_\infty}\right)dy$

λ eddy diffusivity, $\frac{-Q_{turb}}{\partial T/\partial y}$

μ viscosity

ν kinematic viscosity, $\frac{\mu}{\rho}$

ξ dimensionless coordinate parallel to free-stream flow direction, $\frac{x}{l}$

ρ mass density

τ shear in the boundary layer

τ_{turb} turbulent shear in the boundary layer

SUBSCRIPTS

∞ free-stream conditions at element location

t local total conditions, for example, $p_t=p\left(1+\frac{\gamma-1}{2}M^2\right)^{\frac{\gamma}{\gamma-1}}$

$turb$ turbulent

tr transition point

w wall conditions

aw adiabatic wall conditions

g gas other than air

SUPERSCRIPTS

$'$ reference conditions with the T' method, or fluctuating quantities in turbulent flow

$\bar{\ }$ time mean quantities in turbulent flow

$\sim$ dimensionless time mean quantities normalized with respect to the corresponding free-stream quantity, for example, $\tilde{h}=\frac{\bar{h}}{h_\infty}$

CONSTANT-PRESSURE TURBULENT BOUNDARY LAYERS IN DIFFERENT CASES

ANALYSIS OF EQUIVALENCE

The purpose of the analysis which follows is to develop the conditions of equivalence for turbulent boundary layers in different gases with continuum flow. To do this the equations of motion and energy will be expressed in dimensionless form and the resulting dimensionless parameters and boundary conditions studied.

The equations of the constant pressure, steady state, compressible turbulent boundary layer furnish a convenient starting point when put in the following form (ref. 21):

Continuity:

$$\frac{\partial}{\partial x}\left(\bar{\rho}\bar{u}+\overline{\rho' u'}\right)+\frac{\partial}{\partial y}\left(\bar{\rho}\bar{v}+\overline{\rho' v'}\right)=0 \tag{1}$$

x-momentum:

$$\left(\bar{\rho}\bar{u}+\overline{\rho' u'}\right)\frac{\partial \bar{u}}{\partial x}+\left(\bar{\rho}\bar{v}+\overline{\rho' v'}\right)\frac{\partial \bar{u}}{\partial y}=\frac{\partial}{\partial y}\left[(\bar{\epsilon}+\bar{\mu})\frac{\partial \bar{u}}{\partial y}\right] \tag{2}$$

Energy:

$$\left(\bar{\rho}\bar{u}+\overline{\rho' u'}\right)\frac{\partial \bar{h}}{\partial x}+\left(\bar{\rho}\bar{v}+\overline{\rho' v'}\right)\frac{\partial \bar{h}}{\partial y}$$
$$=\frac{\partial}{\partial y}\left[(\bar{\lambda}+\bar{k})\frac{\partial}{\partial y}\overline{T}(\bar{h})\right]+(\bar{\epsilon}+\bar{\mu})\left(\frac{\partial \bar{u}}{\partial y}\right)^2 \tag{3}$$

Equations (1), (2), and (3) can be written in dimensionless form if all quantities are normalized with respect to free-stream quantities (e.g., $\tilde{\rho}=\bar{\rho}/\rho_\infty$, $\tilde{u}=\bar{u}/U_\infty$, etc.):

Continuity:

$$\frac{\partial}{\partial \xi}\left(\tilde{\rho}\tilde{u}+\frac{\overline{\rho' u'}}{\rho_\infty U_\infty}\right)+\frac{\partial}{\partial \eta}\left(\tilde{\rho}\tilde{v}+\frac{\overline{\rho' v'}}{\rho_\infty U_\infty}\right)=0 \tag{4}$$

x-momentum:

$$\left(\tilde{\rho}\tilde{u}+\frac{\overline{\rho' u'}}{\rho_\infty U_\infty}\right)\frac{\partial \tilde{u}}{\partial \xi}+\left(\tilde{\rho}\tilde{v}+\frac{\overline{\rho' v'}}{\rho_\infty U_\infty}\right)\frac{\partial \tilde{u}}{\partial \eta}$$
$$=\frac{1}{Re_l}\frac{\partial}{\partial \eta}\left[(\tilde{\epsilon}+\tilde{\mu})\frac{\partial \tilde{u}}{\partial \eta}\right] \tag{5}$$

where

$$\tilde{\epsilon}=\frac{\bar{\epsilon}}{\mu_\infty}$$

Energy:

$$\left(\tilde{\rho}\tilde{u}+\frac{\overline{\rho' u'}}{\rho_\infty U_\infty}\right)\frac{\partial \tilde{h}}{\partial \xi}+\left(\tilde{\rho}\tilde{v}+\frac{\overline{\rho' v'}}{\rho_\infty U_\infty}\right)\frac{\partial \tilde{h}}{\partial \eta}$$
$$=\frac{1}{Re_l}\frac{\partial}{\partial \eta}\left[\left(\frac{\tilde{\epsilon}}{Pr_{turb}}+\frac{\tilde{\mu}}{Pr}\right)\frac{\partial \tilde{h}}{\partial \eta}\right]$$
$$+\frac{1}{Re_l}\left(\frac{U_\infty^2}{h_\infty}\right)(\tilde{\epsilon}+\tilde{\mu})\left(\frac{\partial \tilde{u}}{\partial \eta}\right)^2 \tag{6}$$

These dimensionless equations are subject to the following boundary conditions on velocity and enthalpy:

$$\tilde{u}(\xi,\ 0)=0 \qquad \tilde{h}(\xi,\ 0)=\tilde{h}_w$$

$$\tilde{u}(\xi,\ \infty)=1 \qquad \tilde{h}(\xi,\ \infty)=1$$

Two turbulent boundary layers will be equivalent (dynamically similar) when the dimensionless differential equations and dimensionless boundary conditions for the two boundary layers are identical. Examination of equations (4), (5), and (6) shows that equivalence can be expected to exist between turbulent boundary layers in different gases when the following dimensionless parameters and variables are matched:

Re_l, U_∞^2/h_∞, $\tilde{h}_w$ — Controllable parameters, required for matching certain coefficients of the differential equations and the boundary conditions on enthalpy.

$\tilde{\rho}(\tilde{h})$, $Pr(\tilde{h})$, $\tilde{\mu}(\tilde{h})$ — State variables, required for matching the thermodynamic state and the laminar transport properties.

$\left(\frac{\overline{\rho' u'}}{\rho_\infty U_\infty}\right)(\xi,\eta)$, $\left(\frac{\overline{\rho' v'}}{\rho_\infty U_\infty}\right)(\xi,\eta)$, $\tilde{\epsilon}(\xi,\eta)$, $Pr_{turb}(\xi,\eta)$ — Turbulence variables, required for matching the eddying motion represented by the fluctuation terms in the differential equations.

As listed above, the parameters and variables are

divided into three groups: the controllable parameters which can be matched by control of test conditions; the state variables which may or may not be matched, depending on the particular thermodynamic and transport properties of a given gas; and the turbulence variables, the matching of which must be determined by experiment. Experimental results are needed since there are available no exact analytical expressions for the turbulence variables which apply through the entire boundary layer. (As a consequence there are no analytical solutions of the system of equations (4), (5), and (6).) Although the turbulence terms can be measured from point to point in comparing two boundary layers, it is probably more convenient simply to measure the over-all effects of these variables on more readily measured quantities such as skin friction and boundary-layer profiles; the latter method is used herein.

In setting up equivalent turbulent boundary layers in two different gases, some of the parameters and variables can be easily matched while the matching of others presents difficulties. The controllable parameters can be exactly matched between two turbulent boundary layers. The three controllable parameters, Re_l, U_∞^2/h_∞, $\tilde{h}_w$, can be thought of as three independent dimensionless energy ratios obtained from six dimensional boundary values, U_∞, h_∞, ρ_∞, μ_∞, h_w, l. The Reynolds number, Re_l, represents the ratio of inertial to viscous energies in the free stream; U_∞^2/h_∞ is double the ratio of kinetic energy to enthalpy in the free stream, while $\tilde{h}_w$ represents the ratio of wall enthalpy to free-stream enthalpy. Even without recourse to the differential equations, it is clear that dynamic similarity between two turbulent boundary layers would not be possible unless these energy ratios were matched.

The matching of the state quantities, $\tilde{\rho}(\tilde{h})$, $Pr(\tilde{h})$, $\tilde{\mu}(\tilde{h})$, depends on the gases being compared.

a. The quantity, $\tilde{\rho}(\tilde{h})$, will be well matched when the gases being compared do not deviate greatly from perfect gases. For thermally perfect gases at constant pressure:

$$\tilde{\rho}(\tilde{h})=\frac{1}{\tilde{T}(\tilde{h})}=\frac{\int_0^{h_\infty}\frac{dh}{C_p(h)}}{\int_0^{h}\frac{dh}{C_p(h)}}\approx\frac{1}{\tilde{h}} \tag{7}$$

If the gases are also calorically perfect:

$$\tilde{\rho}(\tilde{h})=\frac{1}{\tilde{h}} \tag{8}$$

b. The Prandtl number is nearly constant and is approximately the same for all gases in the absence of imperfect gas effects; hence $Pr(\tilde{h})$ will generally be well matched.

c. The dimensionless viscosity, $\tilde{\mu}(\tilde{h})$, is a parameter which, in general, may not be perfectly matched between two different gases. However, this match can be reasonably well approximated by the selection of gases and temperature levels.

There is no effective method of predetermining that the individual turbulence variables can actually be matched at all corresponding points in two boundary layers. However, it is known that if true dynamic similarity exists, the dimensionless differential equations (with boundary conditions) will be identical for two boundary layers. As a consequence, the coefficients of local skin friction, $C_f=\tau_w/(\frac{1}{2})\rho_\infty U_\infty^2$, and the dimensionless velocity profiles, $\tilde{u}(\xi, \eta)$, must be the same for the two boundary layers. (The right-hand side of eq. (5) may be written as $\frac{1}{2}\frac{\partial}{\partial\eta}\left[\frac{\tau}{(\frac{1}{2})\rho_\infty U_\infty^2}\right]$.) By experimentally determining that the C_f's and the dimensionless velocity profiles are identical, it can be concluded that a necessary condition for dynamic similarity has been fulfilled. In the strict sense this is not sufficient to prove dynamic similarity, but one is encouraged to believe that dynamic similarity exists in this case for all practical purposes.

The analysis above has been concerned only with turbulent boundary layers, but it is of interest to note that for dynamic similarity between laminar boundary layers (at zero pressure gradient) in different gases, the quantities that must be matched are the controllable parameters and the state variables as listed above. This may also be seen by inspection of Crocco's equations for the laminar compressible boundary layer (ref. 22).

EQUIVALENCE WITH PERFECT GASES

When specialized for constant-pressure turbulent boundary-layer flows of thermally and

calorically perfect gases, the similarity parameters and variables appear in the following form:

Re_t
$(\gamma-1)M_\infty^2$ } Controllable parameters
$\tilde{T}_w$

$\tilde{\rho}(\tilde{T})$
$Pr(\tilde{T})$ } State variables
$\tilde{\mu}(\tilde{T})$

$\left(\frac{\overline{\rho' u'}}{\rho_\infty U_\infty}\right)(\xi, \eta)$
$\left(\frac{\overline{\rho' v'}}{\rho_\infty U_\infty}\right)(\xi, \eta)$ } Turbulence variables
$\tilde{\epsilon}(\xi, \eta)$
$Pr_{turb}(\xi, \eta)$

Since air is the gas of principal interest, it is convenient to equate the Mach number parameter, $(\gamma-1)M_\infty^2$, for a gas other than air, to the parameter in air and to define an equivalent air Mach number, M_a.

$$(\gamma_g-1)M_g^2=(\gamma_{Air}-1)M_a^2$$

$$M_a=M_g\sqrt{\frac{\gamma_g-1}{\gamma_{Air}-1}} \tag{9}$$

Thus, a gas, g, flowing at an actual free-stream Mach number, M_g, has an equivalent air Mach number, M_a, as defined by equation (9).

It is of interest to consider the validity of the parameter, $(\gamma-1)M_\infty^2$, for flows other than constant-pressure turbulent boundary layers. As noted above, this parameter is valid for either laminar or turbulent boundary layers at constant pressure. It is also valid for comparing two boundary layers with matched dimensionless pressure gradients. However, in this case the dimensionless differential equations must be normalized with respect to constant reference quantities, not to the local free-stream quantities. The parameter, $(\gamma-1)M_\infty^2$, is not valid for external flows. This means that in matching dimensionless pressure gradients around two bodies in external flows, the bodies must, in general, have different shapes.

EQUIVALENCE OF AIR AND HELIUM

If air and helium are considered perfect gases in the constant-pressure turbulent boundary layer, the parameters and terms that must be matched for dynamic similarity are those listed in the previous subsection.

General comparison.—The controllable parameters, Re_t, $(\gamma-1)M_\infty^2$, and $\tilde{T}_w$, can easily be matched between an air and a helium boundary layer. It is of interest to note that for adiabatic boundary layers, the boundary condition on $\tilde{T}_w$ is automatically matched when the Mach number parameter, $(\gamma-1)M_\infty^2$, is matched for gases with equal recovery factors. (As reported in appendix A, the recovery factors for air and helium were found to be essentially the same.) The equivalent air Mach number for a helium flow may be written as (eq. (9)):

$$M_a=M_{He}\sqrt{\frac{\gamma_{He}-1}{\gamma_{Air}-1}}\approx 1.29M_{He} \tag{10}$$

The state variables that should be matched are the quantities, $\tilde{\rho}(\tilde{T})$, $Pr(\tilde{T})$, and $\tilde{\mu}(\tilde{T})$. The dimensionless density, $\tilde{\rho}(\tilde{T})$ is equal to $1/\tilde{T}$ for both air and helium when they are considered perfect gases. The Prandtl number, $Pr(\tilde{T})$, will be approximately matched between air and helium over a considerable temperature range as shown in figure 1. The figure also shows that the Prandtl number for both air and helium varies slowly with temperature over a wide temperature range (refs. 23, 24, 25). (In the regime of continuum flow calculations, the Prandtl number is often taken as

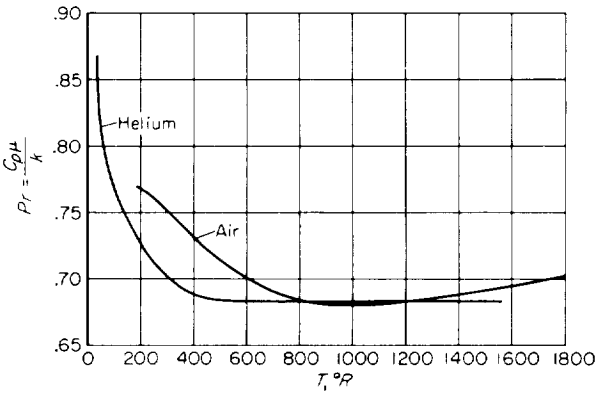

FIGURE 1.—Prandtl numbers of air and helium.

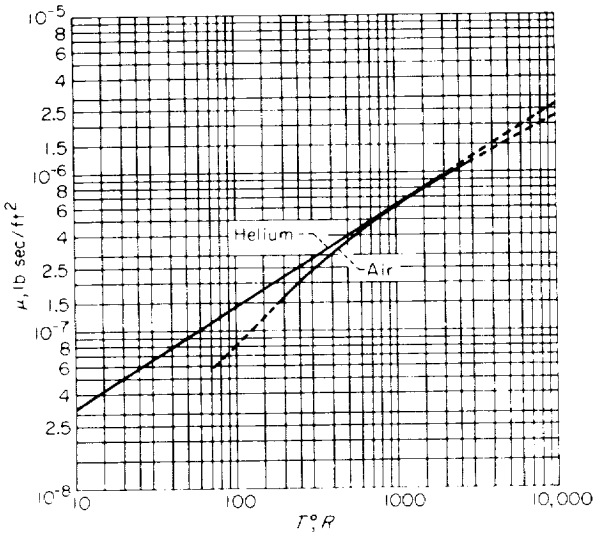

FIGURE 2.—Viscosities of air and helium.

constant.) The dimensionless viscosity, $\tilde{\mu}(\tilde{T})$, cannot be exactly matched between air and helium. Figure 2 shows a logarithmic plot of viscosities of air and helium. The slopes of the curves represent the exponents in a power law for viscosity and indicate the degree of matching of dimensionless viscosities.

For air at high temperatures:

$$\tilde{\mu} \approx (\tilde{T})^{0.6}$$

For air at low temperatures:

$$\tilde{\mu} \approx (\tilde{T})^{0.9}$$

The dimensionless viscosity of helium over a wide temperature range may be closely approximated as:

$$\tilde{\mu} \approx (\tilde{T})^{0.64}$$

It is of interest to observe from the figure that at the higher Mach numbers, the dimensionless viscosity of air at ordinary wind-tunnel temperatures does not perfectly match air at flight temperatures. It is also seen that the dimensionless viscosity of helium matches air at flight temperatures and high Mach numbers better than does air at ordinary wind-tunnel temperatures.

As mentioned in the subsection, Analysis of Equivalence, it is not possible to know in advance whether the turbulence terms,

$$\left(\frac{\overline{\rho' u'}}{\rho_\infty U_\infty^2}\right)(\xi,\eta),\ \left(\frac{\overline{\rho' r'}}{\rho_\infty U_\infty}\right)(\xi,\eta),\ \tilde{\epsilon}(\xi,\eta),\ Pr_{turb}(\xi,\eta)$$

are actually matched between an air and a helium turbulent boundary layer. If dynamic similarity between an air and a helium turbulent boundary layer can be demonstrated experimentally, it should be concluded that the turbulence terms are sufficiently well matched.

Specific comparison.—In attempting to set up equivalent air and helium boundary layers in a wind tunnel, at ordinary wind-tunnel temperature (e.g., $T_t = 600°$ R), one quantity that will have an appreciable mismatch in a portion of the boundary layer is the dimensionless viscosity, $\tilde{\mu}(\tilde{T})$. This mismatch is most serious at the wall (e.g., with $M_a = 4.2$ and $T_t = 600°$ R, $\tilde{\mu}_{w_{\text{Air}}} \approx 1.5\ \tilde{\mu}_{w_{\text{He}}}$). When the dimensionless equations of motion (4), (5), and (6) are considered, it is seen that a mismatch in $\tilde{\mu}(\tilde{T})$ must have some effect on the other quantities, but the magnitude of the effect is difficult to estimate. (In ref. 26 it is predicted that a mismatch in $\tilde{\mu}$ will have a small effect on turbulent skin friction, but a large effect on laminar skin friction.) In equations (5) and (6) the product $(1/Re_l)\tilde{\mu}$ occurs. This can be written

$$(1/Re_l)\tilde{\mu} = (\mu/\mu_w)\tilde{\rho}_w(1/Re_w) \qquad (11)$$

where $Re_w = \dfrac{U_\infty \rho_w l}{\mu_w}$, is the "wall property" Reynolds number. The product $(1/Re_l)\tilde{\mu}$ can be matched in any selected portion of the boundary layer by mismatching Re_l to compensate for any mismatch in $\tilde{\mu}$. It has been thought that $(1/Re_l)\tilde{\mu}$ should be matched somewhere in the sublayer (possibly at the wall) as this should be the region where viscosity is most important. (Away from the wall $\tilde{\epsilon}$ becomes much larger than $\tilde{\mu}$ so that $\tilde{\mu}$ should be less important away from the wall.)

The method of matching $(1/Re_l)\tilde{\mu}$ near or at the wall is easily seen by referring to equation (11). Near the wall μ/μ_w will be nearly unity, hence μ/μ_w will be reasonably well matched regardless of the gas. The dimensionless density $\tilde{\rho}_w$ is matched between two flows being compared at the same M_a and $\tilde{T}_w$. It is, then, necessary to match Re_w in order to secure a good match of $(1/Re_l)\tilde{\mu}$ near or at the wall. This results in a poor match of $(1/Re_l)\tilde{\mu}$ away from the wall (where $\tilde{\mu}$ is possibly not important). The practical question of whether $(1/Re_l)\tilde{\mu}$ should better be matched near the wall or in the free stream can be best answered experimentally by determining whether measured

C_f values correlate with Re_l or Re_w (it either). (Obviously, if there were no mismatch in $\tilde{\mu}$, this question would not arise and it would then be immaterial whether Re_l or Re_w were used in the comparisons.)

In determining the practical equivalence of turbulent boundary layers in air and helium, it will be useful to consider boundary-layer profiles with the variables in several forms. The dimensionless velocity, $\tilde{u}$, may be written as:

$$\tilde{u}=\frac{M}{M_\infty}\sqrt{\tilde{T}}$$

This means that M/M_∞ will be equal at corresponding points in two perfectly equivalent boundary layers. (The M values themselves in the air and helium boundary layers will be in the ratio ≈ 1.29 at corresponding points.) Also, corresponding points in two perfectly matched boundary layers are at equal values of y/θ which can be shown as follows:

$$\frac{y}{\theta}=\frac{\eta l}{\theta}=\frac{\eta l}{(1/2)\int_0^x C_f(x_1)dx_1}$$

$$\frac{y}{\theta}=\frac{\eta}{(1/2)\int_0^\xi C_f(\xi_1)d\xi_1}$$

The relations above are for perfectly matched boundary layers. In view of the mismatch in $\tilde{\mu}$ between air and helium at wind-tunnel temperatures, it is desirable to compare experimental profiles to assess the effect of the $\tilde{\mu}$ mismatch and to assist in determining whether equivalence can be considered to exist for practical purposes.

Profile comparisons can also be made using $u^*=u/u_\tau$ and $y^*=\frac{yu_\tau}{\nu_w}$ as coordinates, with the friction velocity, u_τ, defined as:

$$u_\tau=\sqrt{\frac{\tau_w}{\rho_w}}$$

The quantities, u^* and y^*, as defined, are normalized with respect to wall properties. The equations for u^* and y^* can be written as:

$$u^*=\frac{\tilde{u}}{\sqrt{C_f/2}\sqrt{\tilde{T}_w}}$$

$$y^*=\frac{\eta}{\tilde{\mu}_w}\sqrt{\frac{C_f}{2}}\sqrt{\frac{1}{\tilde{T}_w}}Re_l$$

$$=\eta\sqrt{\frac{C_f}{2}}\sqrt{\tilde{T}_w}Re_w$$

From this it is clear that if two boundary layers are perfectly equivalent (having equal values of C_f and $\tilde{T}_w$ and equal values of $\tilde{u}$ at corresponding points), the quantity, u^*, will be matched at corresponding points. The quantity y^* will be matched at corresponding points if C_f is shown to correlate with Re_w for two boundary layers. On the other hand, if C_f correlates with Re_l for two boundary layers, then the y^* values between air and helium boundary layers will not be matched at corresponding points (at wind-tunnel temperatures) because of the mismatch in $\tilde{\mu}_w$. At a total temperature of 600° R and an M_a value of 4.2 (giving $\tilde{\mu}_{w_{\mathrm{Air}}}\approx 1.5\ \tilde{\mu}_{w_{\mathrm{He}}}$), the mismatch in y^* values will be $y^*_{\mathrm{He}}\approx 1.5\ y^*_{\mathrm{Air}}$ for corresponding points. Experimental profiles showing the variables in the several forms mentioned above should (in addition to skin-friction measurements) assist in determining whether it is better to compare on an Re_l or an Re_w basis.

ADVANTAGES OF USING HELIUM

As is well known, it is difficult to obtain high Mach numbers and high Reynolds numbers simultaneously with air in a wind tunnel. In order to avoid condensation, it is necessary to heat the air, with a resulting loss in density and Reynolds number. It seems desirable, then, to use a gas such as helium that does not condense at the high Mach numbers of interest. As pointed out earlier, helium under wind-tunnel conditions provides a good simulation of air under flight conditions provided imperfect gas effects are not significant. As shown in figure 3, for a given total pressure, higher Reynolds numbers can be obtained at hypersonic Mach numbers with helium than with air in a wind tunnel. As an example, at an equivalent air Mach number of 10, the Reynolds number factor in favor of helium is about 13 to 1. (This factor has a slow dependence on pressure when the total temperature of air is taken as the minimum necessary to avoid condensation at a given Mach number; in figure 3 a total pressure of 1000 psi was used.) This advantage of helium is due to several factors, the principal one being that no

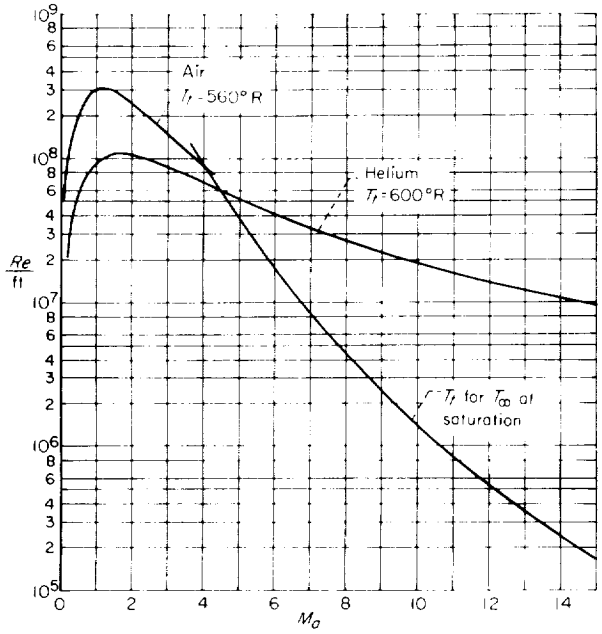

FIGURE 3. Variation of Reynolds number per foot with equivalent air Mach number for air and helium; p_t = 1000 psi.

heating of helium is required. Other factors that contribute to this result are the different ratios of specific heats, and the fact that with equal equivalent air Mach numbers, testing in helium can be conducted at a lower actual Mach number.

APPARATUS AND TEST CONDITIONS

THE 1- BY 10-INCH BOUNDARY-LAYER CHANNEL

The 1- by 10-inch boundary-layer channel was designed to provide high Mach numbers and high Reynolds numbers simultaneously. In figure 4 the test domain of the boundary-layer channel is illustrated in terms of Mach number and Reynolds

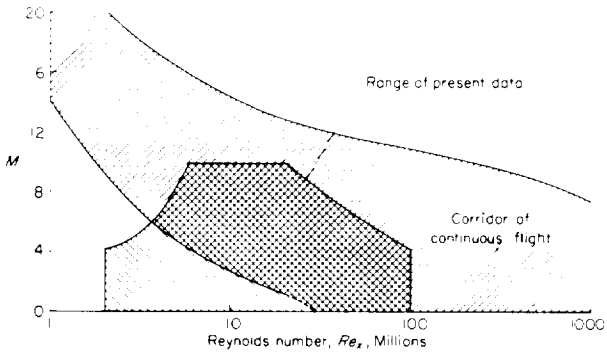

FIGURE 4. -Test domain of the 1- by 10-inch boundary layer channel.

number. For purposes of comparison, also shown is the so-called corridor of continuous flight, which is the approximate Mach number Reynolds number range for continuous, sustained flight of airplanelike vehicles. (A characteristic length of 50 feet was used in the calculation; the upper bound of the corridor was taken at an equilibrium surface temperature of 2000° F, and the lower bound was estimated using a dynamic pressure of 100 psf.) Most previous skin-friction data were taken in the area to the left and below the lower boundary of the corridor of continuous flight. It is seen that the boundary-layer channel has extended the Mach number Reynolds number range into a regime of considerable interest. In order to cover the range shown, air was used as the working fluid up to a Mach number of 4.2, and helium was used from equivalent air Mach numbers of 4.2 up to 9.9.

A sketch of the equipment layout is shown in figure 5; figure 6 is a schematic drawing of the test region; and figure 7 is a photograph of the equipment. Although this apparatus is called a channel (because of its dimensions), the series of tests being reported were not for channel flows. During the present series of tests, there was always a core of potential flow between the top and the bottom boundary layers.

The 1- by 10-inch boundary-layer channel is a blowdown type wind tunnel. The gas used as a working fluid is stored at 2400 psi in two 40,000 cubic foot capacity gas trailers. As shown in figure 5 the gas flows from the trailers through the inlet line into the heat exchanger, and then into the settling chamber of the tunnel at the desired temperature and pressure. The total pressure (measured in the settling chamber) was controlled by valves near the trailers. The total temperature was controlled by means of a heat exchanger consisting of a thermal mass of 3,000 pounds of copper tubes. All heating of the thermal mass was performed prior to running in order to preset the desired total temperatures. Runs were terminated when the heat exchanger could no longer maintain the preset total temperature. In the present series of tests the total temperature was preset relative to the ambient wall temperature in the tunnel test section so that the boundary layers were adiabatic at the walls. This procedure gave total temperatures for all runs of approximately 600° R. (See appendix A.)

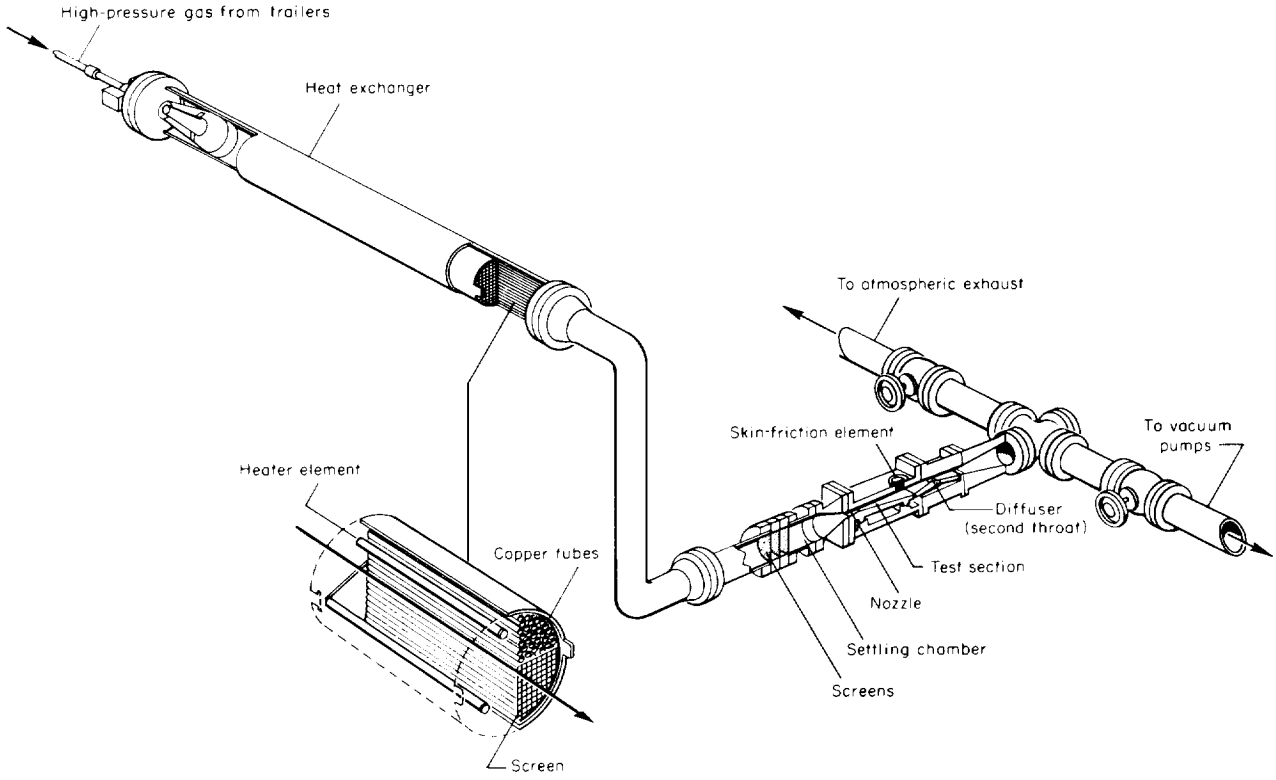

FIGURE 5.—Schematic drawing of boundary-layer channel and associated equipment.

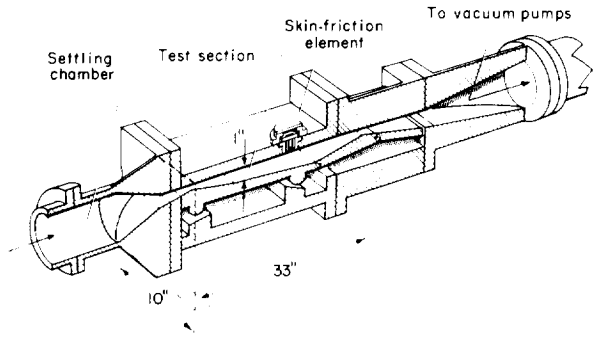

FIGURE 6.—Details of test region of boundary-layer channel.

The tunnel dimensions (fig. 6) were designed to give an essentially two-dimensional flow. The top plate of the tunnel is completely flat; the nozzle contouring is entirely on the bottom wall. Four interchangeable nozzles were used, three contoured for supersonic flows and one (a flat plate) for subsonic flows. Mach number and pressure gradient settings were made by the selection and adjustment of the interchangeable nozzle blocks. Reynolds number control was obtained by varying the total pressure for a given tunnel geometry.

As shown in figure 5, the apparatus has two exhaust routes available, atmospheric and vacuum. During supersonic running, the exhaust was always to the vacuum exhaust system. An optimum compression ratio was achieved by means of an adjustable second throat. The atmospheric exhaust was used for subsonic running. For the subsonic runs, Mach number control was obtained with the (supersonic) diffuser throat operating as a sonic choke downstream of the test section.

In the series of tests conducted, the Mach number and Reynolds number were varied to the limits of the present capability of the equipment. The upper limit of the Mach number (and the lower limit of the Reynolds number at a given Mach number) were determined by the exhaust system back pressure (compression ratio available), while the maximum Reynolds numbers were dictated by safety considerations. The maximum settling chamber pressure was 700 psig for supersonic flows and 310 psig for subsonic flows.

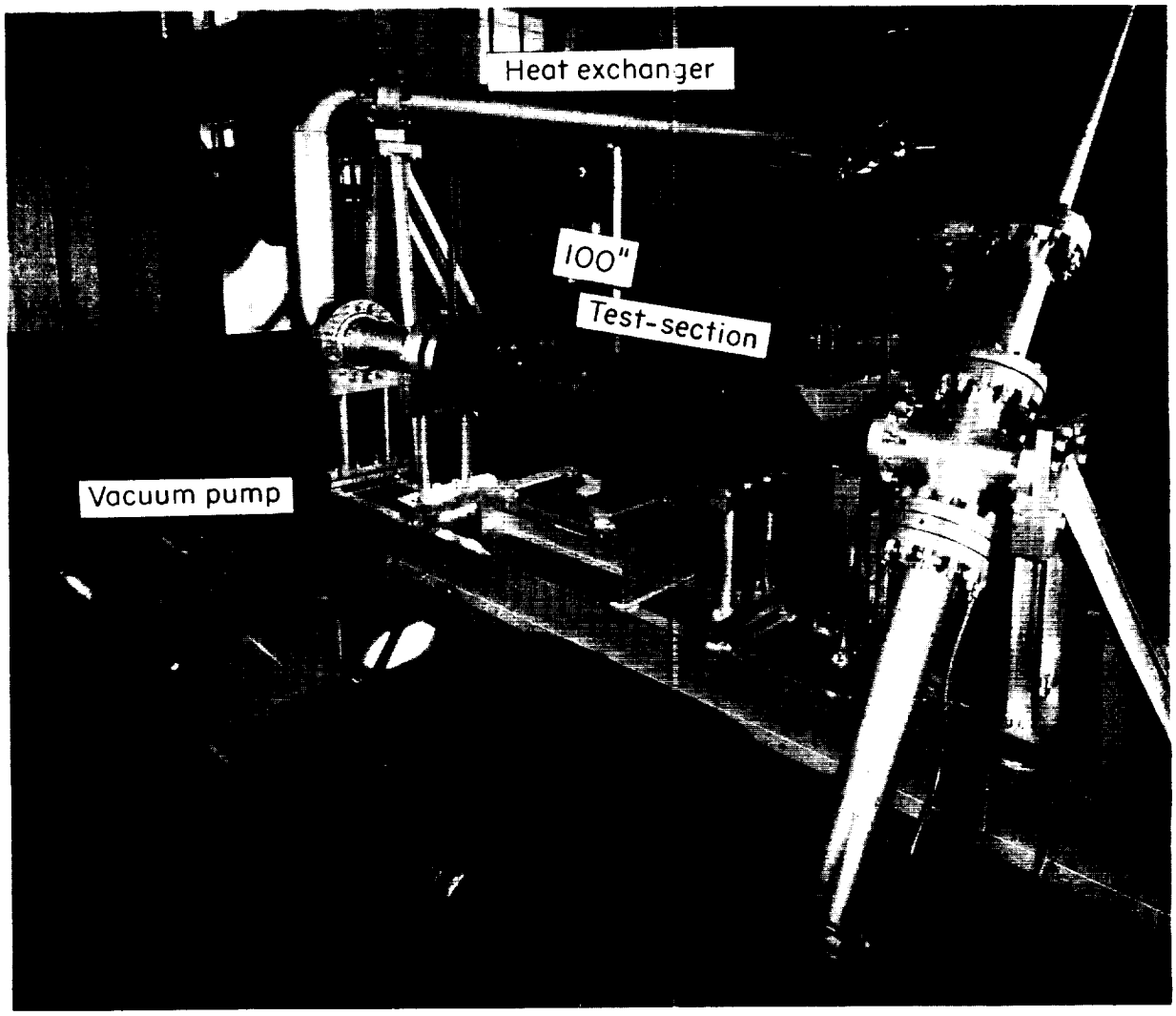

FIGURE 7.—The 1- by 10-inch boundary-layer channel without instrumentation.

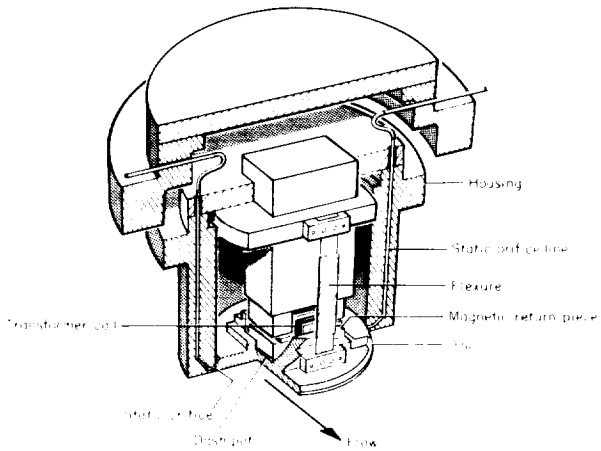

FIGURE 8.—Skin-friction element.

SKIN-FRICTION ELEMENT

Local skin friction was measured directly by means of the skin-friction element shown in figures 8 and 9. The element consisted of a disk 2¼ inches in diameter suspended from two flexures. The streamwise force on the disk was measured by means of a differential transformer. The transformer itself maintained a fixed position while two iron magnetic return pieces on the disk completed the magnetic circuit. All of the metal parts of the element not in the magnetic circuit were made of K-monel. In the neutral position, the gap between the disk and its housing was 0.005 inch. The element had no nulling device and simply deflected under load.

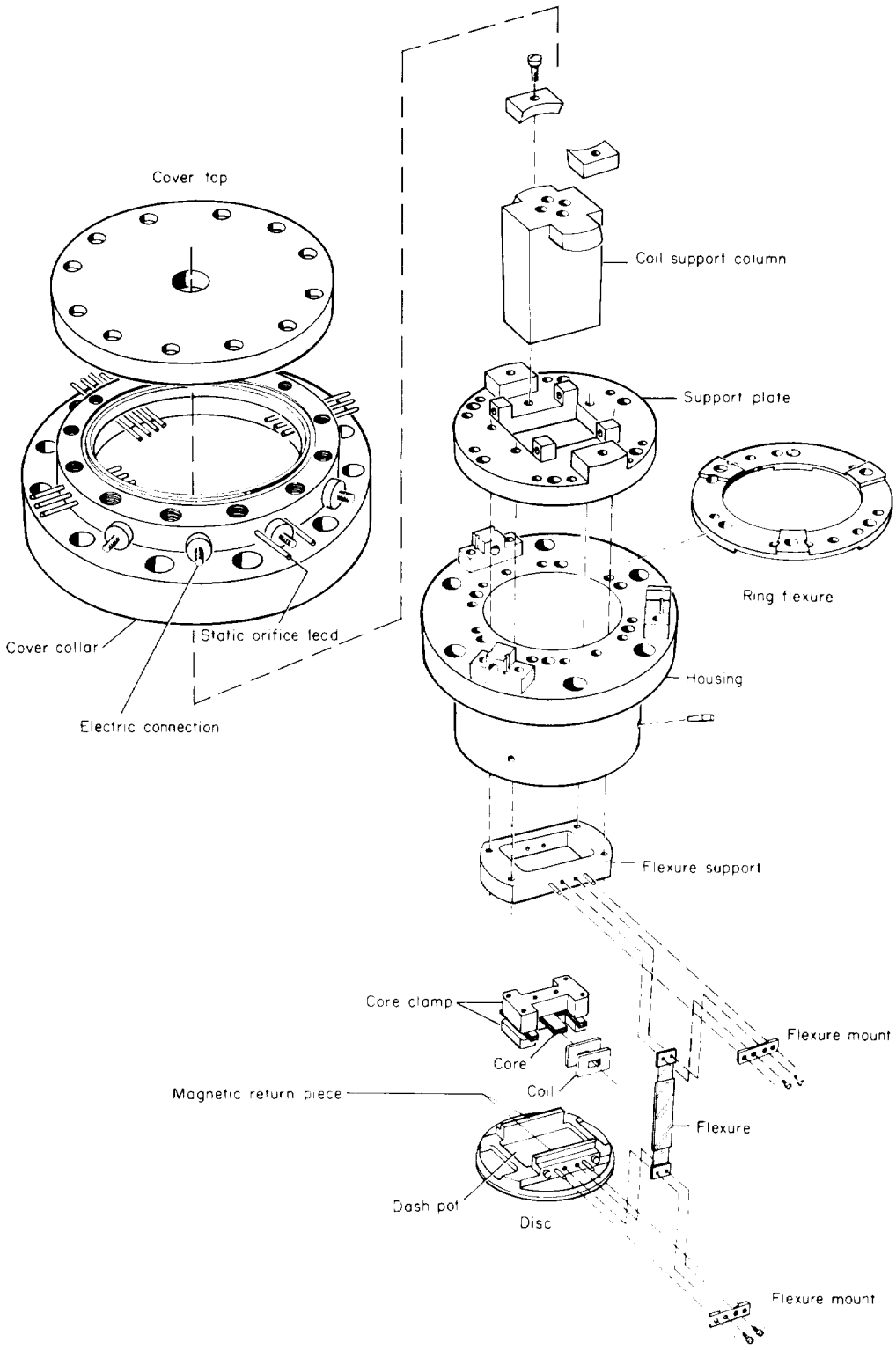

FIGURE 9.—Exploded view of skin-friction element.

The top face of the disk was formed as a dash pot which contained 1000 centistoke silicone oil as a damping fluid. The disk in its mounting was electrically insulated from the element housing so that an electric fouling meter could be used to indicate contact between the disk and the housing. The mounts for the flexures constrained the ends of the flexures to remain parallel and vertical. This meant that the disk was constrained to remain parallel to its no-load position (horizontal). Interchangeable pairs of flexures were calibrated and used for different loading ranges. The approximate force at a full load deflection of approximately 0.005 inch for the pair of flexures used for most of the tests was 0.1 pound. The disk was determined to be flush with its housing to within 10 microinches by means of an optical interferometer. Subsequent tests to determine flushness requirements showed that for a Mach number of 4.2, the element disk could be displaced as much as 200 microinches in or out of the housing with no noticeable change in skin friction. The surface of the disk was finished to 2 microinches, the housing to 4 microinches, while the top plate of the channel was finished to 15 microinches. These finishes were selected to provide "hydraulically smooth" surfaces over the range of variables tested. The finishes on the disk and housing were measured by means of optical flats and on the top plate by means of a profilometer. Twelve static orifices in the gap surface of the housing surrounding the disk provided pressure data for calculating the buoyancy force on the disk. These pressures were read on a small manometer board near the element which used 10 centistoke silicone oil.

The output of the differential transformer was fed into a bridge circuit servo with a digital readout. The electrical circuitry is shown in figure 10. The calibration of the element and servo combination showed a repeatability of 0.1 percent of the full load reading and was nearly linear over the full range (departed approximately 2 percent from linearity at full load). Over the range of temperatures used, the temperature effect on the calibration was almost negligible. (Calibration curves taken at 40° F and 83° F showed a slope difference of approximately ¼ percent.) A description of the electrical circuitry of the element and servo is given in appendix B.

GENERAL INSTRUMENTATION

Static-pressure distributions were obtained through orifices in the top plate of the tunnel (fig. 11). The orifices were connected to a 30-tube manometer board that used 10 centistoke silicone oil and was referenced to a near vacuum. The

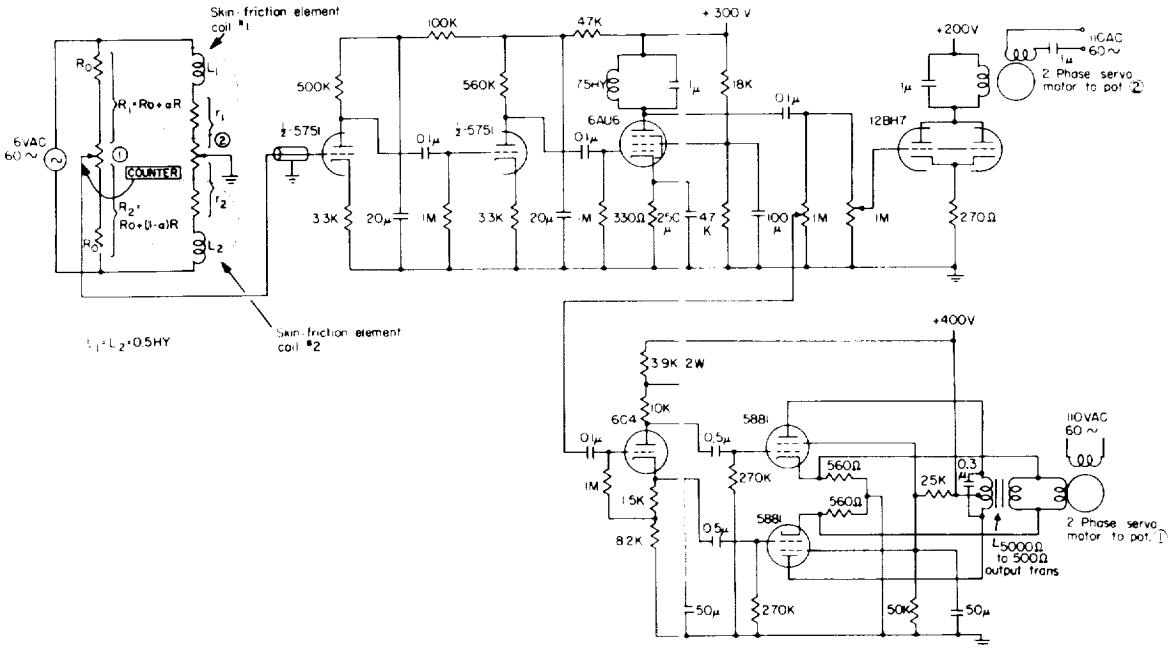

FIGURE 10.—Circuitry of skin-friction element and servo.

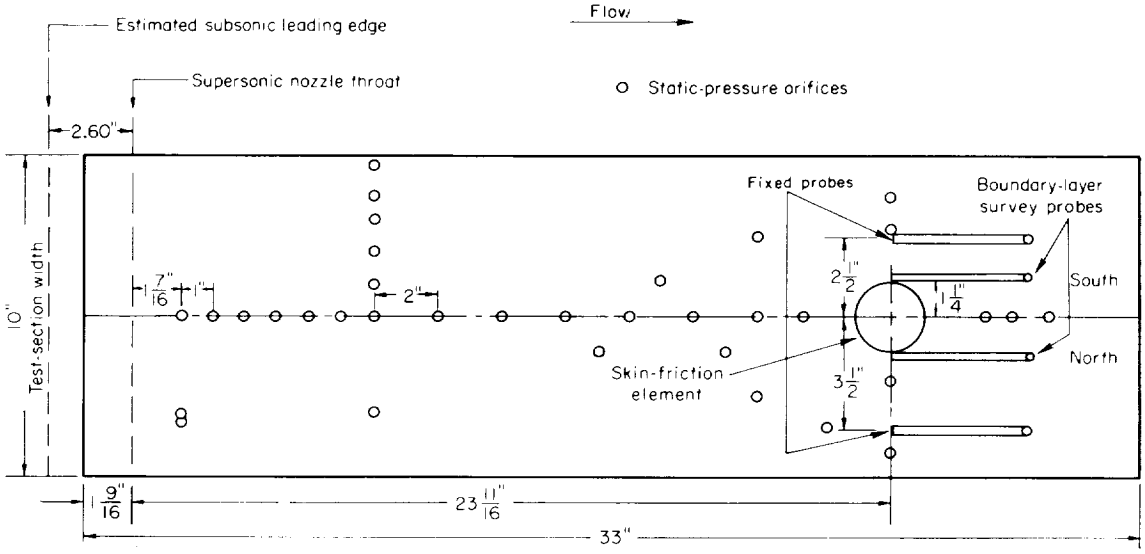

FIGURE 11.—Plan view of test-section top plate.

total pressure was measured at the settling chamber with a Bourdon gage. Impact pressures in the potential flow core were measured by two fixed probes connected to pressure transducers which were electrically connected to bridge-type servos with digital readouts. Boundary-layer impact pressures were measured by two movable probes connected to pressure transducers, and located 1¼ inches on either side of the element center line. The boundary-layer probes were flattened tubes with an inside height of 0.002 inch, an outside height of 0.004 inch, and a width of 0.045 inch. The traversing of the probes was controlled remotely and could be positioned to within 0.002 inch.

Temperatures were measured at 17 locations including the settling chamber, the skin-friction element, several locations and depths in the top plate, the manometer boards, and the heat exchanger. Iron constantan thermocouples with self-balancing potentiometers were used. The settling chamber temperature was continuously recorded.

PROCEDURE AND DATA REDUCTION

Tests conducted were of three types: skin-friction tests, transition tests to determine the virtual origin of the turbulent boundary layer, and boundary-layer surveys.

SKIN-FRICTION TESTS (AIR AND HELIUM)

Skin-friction tests in air were performed at both subsonic and supersonic Mach numbers while the tests using helium as the working fluid were made at supersonic Mach numbers only. The quantities directly measured were: the force on the skin-friction element, the total pressure (in the settling chamber), impact pressures (usually 2) in the potential flow core near the element, the static pressure at the skin-friction element, 12 buoyancy pressures around the element disk, 30 static pressures on the top plate of the test section, the total temperature (in the settling chamber), and other temperatures of interest.

The free-stream Mach number, M_∞, and the dynamic pressure, q_∞, were obtained from the measured static and total pressure and the usual isentropic flow equations. The existence of an isentropic core was verified by a comparison of impact pressures calculated from isentropic and shock relations with measured impact pressures. These pressures agreed within 4 percent.

In the determination of Reynolds number, the length used was from the virtual origin of the turbulent boundary layer. The determination of the virtual origin is discussed in the following subsection. For the viscosity of air (fig. 2),

Sutherland's formula in the following form was used (refs. 27 and 28):

$$\mu=2.270\frac{T^{3/2}}{T+198.6}\times10^{-8}\text{ lb sec/ft}^2 \qquad (12)$$

For helium, in the temperature range at which tests were run, the viscosity-temperature relationship used was (fig. 2):

$$\mu=7.35T^{0.64}\times10^{-9}\text{ lb sec/ft}^2 \qquad (13)$$

This formula is based on a faired curve through available experimental data (ref. 24).

The buoyancy force on the disk of the skin-friction element was obtained by numerically integrating the streamwise component of forces due to the pressures acting on the effective projected area of the disk. The following sketch shows the disk dimensions and orifice locations:

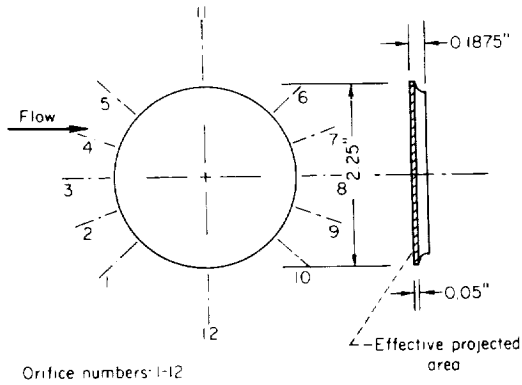

Defining the buoyancy force, F_{buoy}, as positive in the upstream direction, and defining F_{total} as the total force sensed by the disk of the skin-friction element, one can write:

$$\tau_w A=F_{skin\ friction}=F_{total}+F_{buoy}$$

where A is the flat surface area of the disk. The experimentally obtained ratio of the buoyancy force to the skin-friction force, $F_{buoy}/F_{skin\ friction}$, as a function of Reynolds number for the various Mach numbers used is shown plotted in figure 12. It is seen that the buoyancy forces were relatively small except for the case with $M_a=6.7$ (see subsection below entitled Accuracy). The coefficient of local skin friction, C_f, is given by the defining equation:

$$C_f=\frac{\tau_w}{q_\infty} \qquad (14)$$

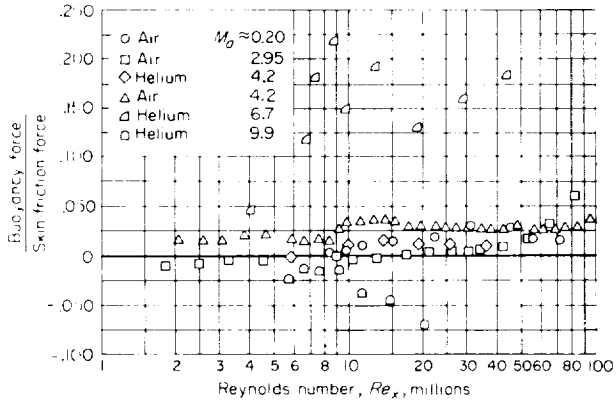

FIGURE 12.—Relative magnitude of buoyancy force on skin-friction element.

Tests at a given Mach number were conducted with a fixed nozzle and test-section geometry. Consequently, there was a slight variation in Mach number with Reynolds number as a result of the variation in boundary-layer thickness as shown in figure 13. In order to present skin-

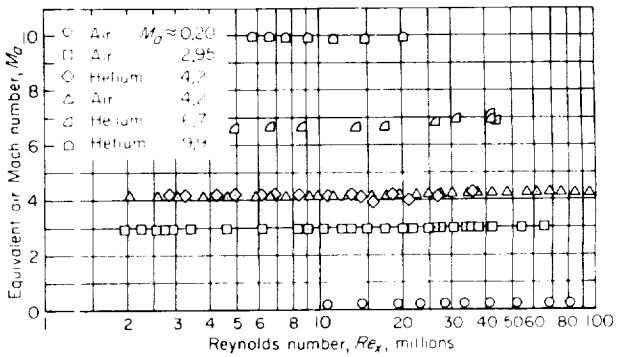

FIGURE 13.—Variation of tunnel Mach number with Reynolds number for various nozzle settings.

friction results at fixed values of Mach number, the measured skin-friction coefficients were corrected by means of the following expression:

$$\Delta C_f=\left(\frac{\Delta C_f}{\Delta M_\infty}\right)\Delta M_\infty$$

Although the factor $(\Delta C_f/\Delta M_\infty)$ could have been determined by experiment, it was more conveniently determined by the T' method (ref. 19). Any errors introduced by this procedure are unimportant since the corrections were always less than 1 percent.

TRANSITION TESTS TO DETERMINE THE VIRTUAL ORIGIN

As noted previously, the length used in the calculation of Reynolds numbers was taken from the approximate location of the virtual origin of the turbulent boundary layer to the center of the skin-friction element. In locating the virtual origin for supersonic flows, it was elected to determine the point of maximum local skin friction, which is known to be near the point of transition (ref. 29). The point of maximum local skin friction was determined by means of impact probes at the wall. These probes were hollow needles of 0.020 inch diameter with a slot of height 0.002 inch for pressure-sensing. The needles were fitted in the top plate static orifices and were adjusted so that the slot just cleared the wall surface. The impact probes at the wall were located in fixed positions on the top plate and the total pressure was varied. It can be shown that:

$$C_f \approx \frac{k\sqrt{\Delta p}}{p_t^{3/2}}$$

where Δp is the difference between the impact pressure sensed by the probe and the local static pressure, p_t is the settling chamber pressure, and k is a proportionality constant. This crude approximation was adequate for the purpose used; it was not necessary to calibrate the probes, since the only interest was in knowing whether the boundary layer was laminar, turbulent, or in transition. For each x-station at which the probes were placed, a plot was obtained as illustrated in the following sketch:

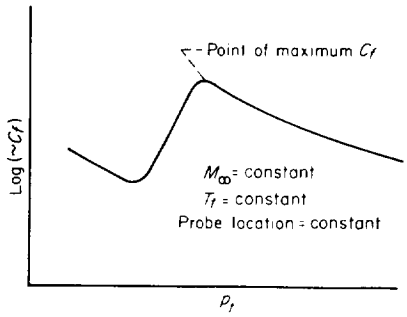

From the group of plots typified by the sketch above, a plot was made (for each Mach number) showing the location of the point of maximum local skin-friction as a function of the total pressure. This type of plot is illustrated in the following sketch:

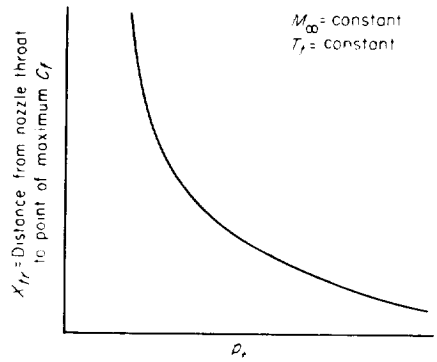

With decreasing total pressure, p_t, the point of transition moves downstream and eventually reaches the element itself. Data were not reduced or reported where transition was completed at a distance closer than 8 inches upstream of the element's center. This distance corresponded to approximately 4 disk diameters or to a minimum of approximately 12 boundary-layer thicknesses. This distance limitation was selected because it was felt that the turbulent boundary layer was probably not in equilibrium (free from historical effects) over shorter distances. Another factor in selecting an 8 inch minimum length of run was that the disk diameter was required to be small relative to the length of run of the turbulent boundary layer, inasmuch as the coefficient of local skin friction as calculated and reported was actually an average value over the disk area.

In order to have a convenient method for converting from Re_L to Re_x, the data typified by the preceding sketch were replotted into a working plot in figure 14 with Re_L as abscissa, and Re_x/Re_L as ordinate. The ordinate is thus a factor to be multiplied by Re_L, to obtain the Reynolds number measured from the virtual origin, Re_x. The dotted extensions of the curves are extrapolations based on a constant Reynolds number of transition which was taken as the value obtained at the farthest upstream station at which measurements were made. These Reynolds numbers are as indicated in the figure. It is seen in figure 14 that the Reynolds number factor is nearly unity at the higher Reynolds numbers. This means that with supersonic flow at high Reynolds numbers the virtual origin was close to the nozzle

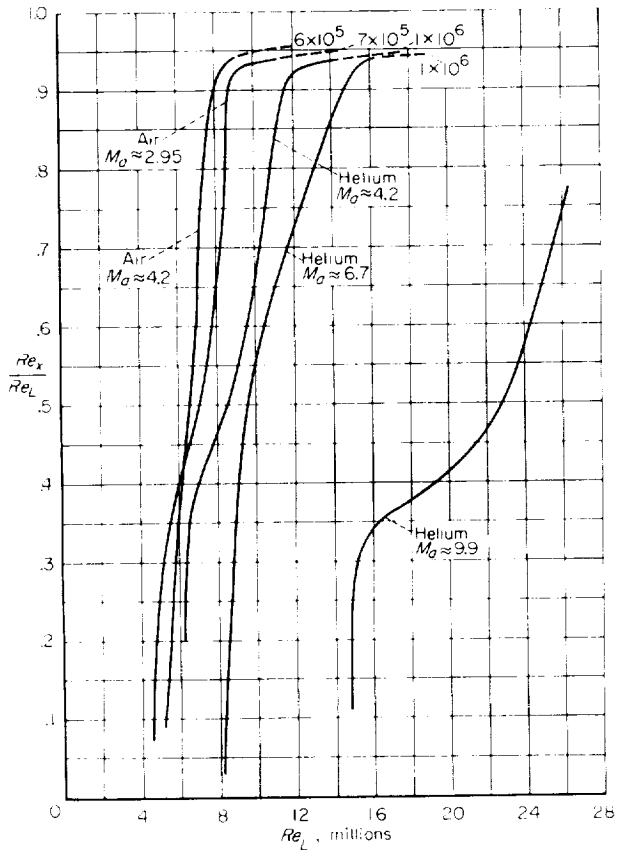

FIGURE 14.—Factor for determining Reynolds number measured from the virtual origin.

throat. Except at $M_a=9.9$, the great bulk of skin-friction data were obtained at Reynolds numbers greater than shown on figure 14. For these cases Re_x was obtained by subtracting from Re_L the Reynolds number of transition (as labeled at the tops of the curves).

With subsonic flow, a different procedure was used for obtaining the virtual origin. The probe technique described above showed that, at the Reynolds numbers of interest, transition occurred ahead of the orifice farthest upstream in the top plate. For calculations of Reynolds number, the point of transition was taken to be the junction of the sharply converging transition section (fig. 6) and the flat plate section. This point was 2.60 inches upstream of what would have been the location of the nozzle throat for supersonic runs (fig. 11).

BOUNDARY-LAYER SURVEYS

Boundary-layer surveys at the longitudinal position of the skin-friction element were obtained at each of the supersonic Mach numbers and at selected Reynolds numbers. The surveys were performed by the usual method of pitot traversing. Frequently two surveys were taken simultaneously, one on each side of the skin-friction element. The momentum thickness, θ, was obtained from the defining equation (see symbols) by graphical integration. Constant static pressure, constant total temperature (settling chamber temperature), and constant specific heats across the boundary layer were assumed in the calculation of u and ρ through the boundary layer and of θ. In the calculations of $u^*=\frac{u}{u_\tau}$ and $y^*=\frac{yu_\tau}{\nu_w}$, the friction velocity was calculated as $u_\tau=\sqrt{\frac{\tau_w}{\rho_w}}$, where τ_w was measured by the skin-friction element.

ACCURACY

An effort was made to use procedures that would give the best possible accuracy of data from the equipment. To keep random errors within small bounds, skin-friction measurements with air were repeated five times, and data with helium, three times. The scatter of the C_f data indicated a probable random error of approximately 2 percent. Possible sources of systematic errors arose from the correction for the buoyancy force, from the effects of a small or irregular pressure gradient, and in the calculation of Reynolds number. The contributions of these systematic errors will be considered in the estimate of the over-all accuracy of C_f.

An error in the buoyancy force correction could have been introduced through not knowing exactly the effective area on which the buoyancy pressures acted, and in not knowing the buoyancy pressure over every infinitesimal element of area. It is estimated that the buoyancy force is in error by less than 10 percent. Since the buoyancy force was generally less than 5 percent of the skin-friction force, and never more than 22 percent (fig. 12), the error in the skin-friction coefficient due to buoyancy force error is probably less than 2 percent. As a check on this, a number of skin-friction tests were run at a Mach number of 4.2 using a disk in the skin-friction element with a side projected area of four times that used in the regular tests. This disk gave buoyancy forces that were approximately 20 percent of the skin-friction force, but the skin-friction coefficients obtained

with the two disks checked each other within 2 percent. From this experience, it is believed that the buoyancy forces at a Mach number of 6.7 were not excessive. (The irregularity of the buoyancy force trend at this Mach number shown in figure 12 is believed to be due to a slight wave pattern in the flow.)

The deviations of static pressure from zero pressure gradient as obtained in typical tests are shown in figure 15. The small wave pattern at $M_a=6.7$ can be seen. Also shown is a small favorable pressure gradient at $M_a=2.95$. Deviations

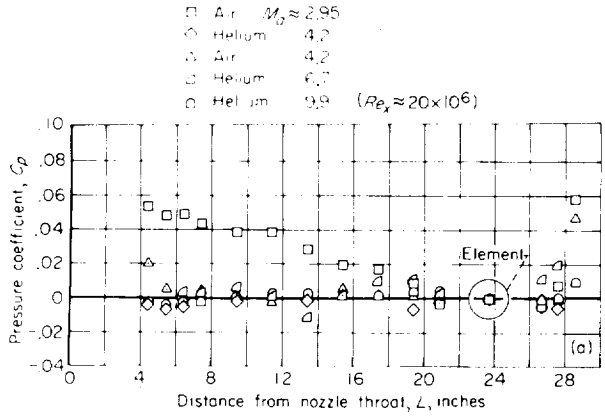

(a) Longitudinal pressure distributions.

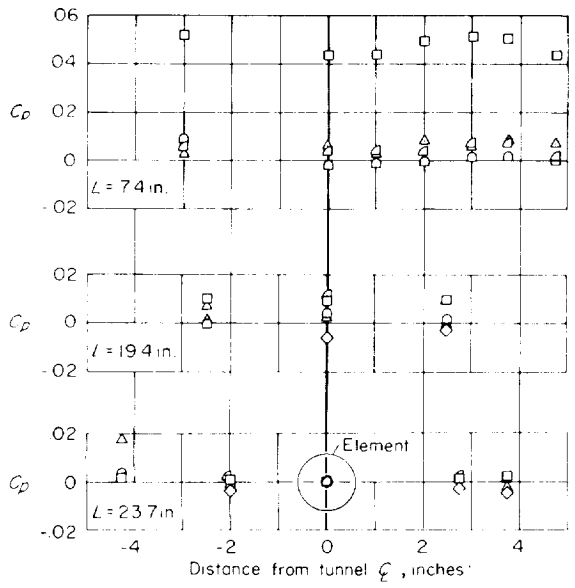

(b) Transverse pressure distributions at various distances, L, from nozzle throat.

FIGURE 15.—Typical static-pressure distributions for $Re_x \approx 26\times10^6$.

from zero pressure gradient of these amounts were used in a special series of tests at $M_a=4.2$ in order to determine the effect of small pressure gradients. It was found that the change in C_f from the zero pressure gradient case was less than the small scatter of the data. It is believed that all of the data have a probable error in C_f due to pressure gradient of less than 2 percent.

Errors in the calculation of Reynolds number would have been almost entirely due to errors in estimating the location of the virtual origin. The true location of the virtual origin was probably slightly upstream of the point of maximum C_f, which was used for supersonic flows. It seems almost certain that the virtual origin for supersonic flows was never upstream of the nozzle throat. (In any case the boundary layer had to be very thin at the nozzle throat.) With supersonic flows at the highest Reynolds numbers, the point of maximum C_f (except at $M_a=9.9$) was close to the nozzle throat (fig. 14). It is believed that the probable error in Reynolds number must have been appreciably less than the quantity, $1-(Re_x/Re_L)$ (fig. 14). The probable error in Reynolds number, then, is small for data at Reynolds numbers near the upper ends of the curves in figure 14 (except at $M_a=9.9$). As noted previously the bulk of skin-friction data were obtained at Reynolds numbers greater than shown in figure 14 (except at $M_a=9.9$), so that probable error in Reynolds number for all these data must have been small. With decreasing Reynolds numbers the quantity, $1-(Re_x/Re_L)$, and hence the probable error becomes progressively greater. Data with a turbulent boundary-layer length between 8 and 14 inches ($0.34<Re_x/Re_L<0.60$) are shown with flagged symbols in the skin-friction plots to denote that these data are not as accurate as the higher Reynolds number data. As mentioned previously, data with a turbulent boundary length of less than 8 inches ($Re_x/Re_L<0.34$) are not reported. At Mach numbers other than 9.9 it is estimated that for the unflagged data ($Re_x/Re_L>0.60$) the probable errors in Reynolds number are less than 6 percent at the highest Reynolds numbers and less than 25 percent at the lowest Reynolds numbers. At $M_a=9.9$, these probable errors are estimated to be less than 15 and 25 percent, respectively. Since the slope of a plot of log C_f against log Re_x is approximately $-1/5$, these errors correspond approximately to errors in

C_f of 1 and 5 percent at Mach numbers other than 9.9, and 3 and 5 percent at M_a=9.9.

With subsonic flows, at the Reynolds numbers tested, the virtual origin was upstream of the farthest upstream orifice in the top plate. It is believed that the virtual origin was not upstream of the point assumed (beginning of the flat-plate section) by any large amount since this would have put the virtual origin in a rapidly converging transition section (fig. 6). It is estimated that the probable error in Reynolds number for subsonic flows was less than 15 percent. This would correspond to a probable error in C_f of approximately 3 percent.

It is estimated that, for all Mach numbers, the total probable error in the measured skin-friction coefficients is less than 5 percent at the highest Reynolds numbers and less than 6 percent at the lowest unflagged Reynolds numbers. No attempt has been made to estimate the accuracy of the flagged points. With decreasing Reynolds numbers, these points become progressively less accurate and tend to become erratic, as noted below in the section, TEST RESULTS AND DISCUSSION. The fact that the best accuracy is obtained at the highest Reynolds numbers is probably fortunate, since the highest Reynolds numbers are in the regime of greatest interest.

Probable errors in boundary-layer thickness or momentum thickness are estimated to be equivalent to errors in Reynolds number and thus to have approximately the same probable errors as Reynolds number. The probable error in θ, then, becomes greater at the lower Reynolds numbers. In some cases simultaneous profiles were taken on either side of the skin-friction element. Spanwise variations in θ averaged approximately 12 percent and it is believed that transverse variations in the virtual origin location existed across the test section width. The maximum spanwise variation in θ was 14 percent and occurred at a low Reynolds number with a rapidly shifting virtual origin (fig. 14).

TEST RESULTS AND DISCUSSION

The data presented show the effects of Mach number and Reynolds number on local skin friction with adiabatic conditions at the wall. The effect on the coefficient of local skin friction of varying the wall temperature was not included in the scope of the present series of tests. Since this effect can be large under certain conditions (ref. 19), the data as presented, should not be used directly to estimate the coefficient of local skin friction in a nonadiabatic boundary layer.

EXPERIMENTAL DETERMINATION OF THE EQUIVALENCE OF AIR AND HELIUM IN THE TURBULENT BOUNDARY LAYER

The purpose of the first phase of the testing program was to evaluate the equivalence of air and helium in the turbulent boundary layer. This was clearly necessary prior to setting up an extensive testing program using helium at the higher Mach numbers. The evaluation of equivalence was made from comparisons of skin friction and profiles for boundary layers in air and helium. The air boundary layer was at a free-stream Mach number of approximately 4.2, whereas the helium boundary layer was at an actual free-stream Mach number of approximately 3.25, or at an equivalent air Mach number, M_a, of approximately 4.2. Since this comparison is between helium and air at wind-tunnel temperatures ($T_t \approx 600°$ R), there is the previously discussed mismatch in $\tilde{\mu}(\tilde{T})$ between the two gases in the boundary layers (at the wall, $\tilde{\mu}_{w_{\mathrm{Air}}} \approx 1.5\ \tilde{\mu}_{w_{\mathrm{He}}}$).

Figure 16 shows the comparison of skin-friction results obtained. In figure 16(a) the comparison is made between skin friction for air and helium boundary layers as a function of the Reynolds number based on free-stream viscosity and density, Re_x (which is the same as Re_l at the skin-friction element). It is seen that the local skin-friction coefficients for air and helium fall on essentially one curve. In figure 16(b), where the same comparison is made as a function of the Reynolds number, Re_w, based on wall viscosity and density, the helium points fall a few percent above the air points, but the agreement is still reasonably good. Although the reasons for it are not known, it seems clear that the skin-friction data correlate slightly better when Reynolds number is based on free stream rather than on wall properties. Consequently, the free-stream Reynolds number is used in the subsequent figures.

Boundary-layer profiles for both air and helium at an equivalent air Mach number of 4.2 and at equal values of the free-stream Reynolds number are compared in figure 17. The profiles were determined from surveys taken near the skin-

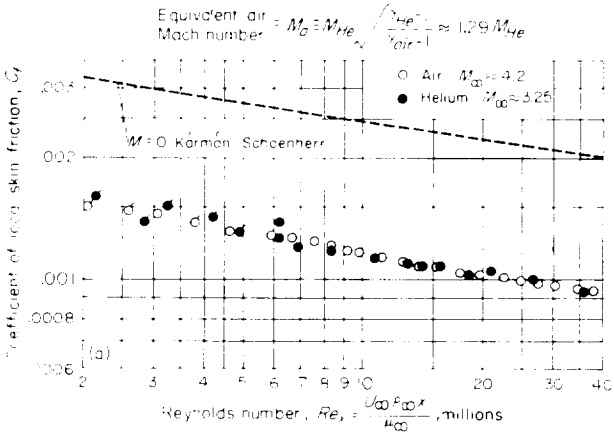

(a) Comparison using Reynolds number based on free-stream properties, Re_x.

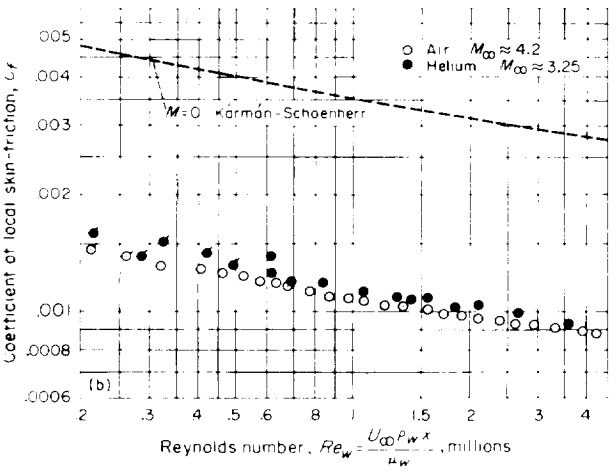

(b) Comparison using Reynolds number based on wall properties, Re_w.

FIGURE 16.—Equivalence of air and helium turbulent skin friction.

friction element. In some cases the profiles were determined from surveys made simultaneously on either side of the element. Data from these surveys are shown plotted in figure 17 (a) and (b) and are labeled north probe and south probe. An average obtained between the probes is given in figure 17(c). It was reasonable to use this average since the friction velocity, u_τ, was calculated from the shear sensed by the skin-friction element (which was not at the exact location of either probe).

The data in figure 17 show that the air and helium profiles are almost identical. In parts (a) and (b) of the figure, the small differences appear primarily in the portions of the profiles near the wall. This is not surprising since with equal free-stream Reynolds numbers there is a mismatch near the wall in the dimensionless viscosities of air and helium. In part (c) of the figure the differences are greatest near the edge of the boundary layer. This is a consistent result with that of parts (a) and (b) because in part (c), y^* has been normalized on the basis of a wall quantity, u_τ, and differences in the profiles should show up most prominently away from the wall. Although the air and helium profiles are very nearly the same, the calculated values of the momentum thickness, θ, do not correlate perfectly as shown by the tabulation in figure 17. This variation in θ is of the same order as the traverse variation in θ obtained between the north and south probes and is considered to be equivalent to a probable error in the evaluation of Reynolds number, as noted previously.

Despite the calculated differences in θ values, the data presented in figures 16 and 17 are considered to form an experimental verification of the equivalence of air and helium in the constant pressure turbulent boundary layer. The good agreement between C_f values, in spite of the mismatch of $\tilde{\mu}(\tilde{T})$, indicates that the turbulent skin-friction coefficient is not overly sensitive to variations in $\tilde{\mu}(\tilde{T})$. This further implies that values of turbulent C_f in air are not particularly sensitive to the temperature levels of the air and that wind-tunnel data taken with air should be practically valid for air in flight (with continuum conditions). At the higher Mach numbers, wind-tunnel data taken with helium should be valid for air in flight since the $\tilde{\mu}(\tilde{T})$ match between helium and flight air is better than the match between helium and wind-tunnel air.

SKIN-FRICTION RESULTS

Using the concept of the equivalence of air and helium in the turbulent boundary layer, skin friction data were taken with air up to an equivalent air Mach number of 4.2 and with helium at the higher equivalent air Mach numbers. The results, presented in several ways, are summarized in figures 18 through 21, inclusive. Each curve is labeled with its appropriate equivalent air Mach number, M_a.

As previously discussed, the coefficient of local skin friction should be determined as a function of the Reynolds number measured from the virtual

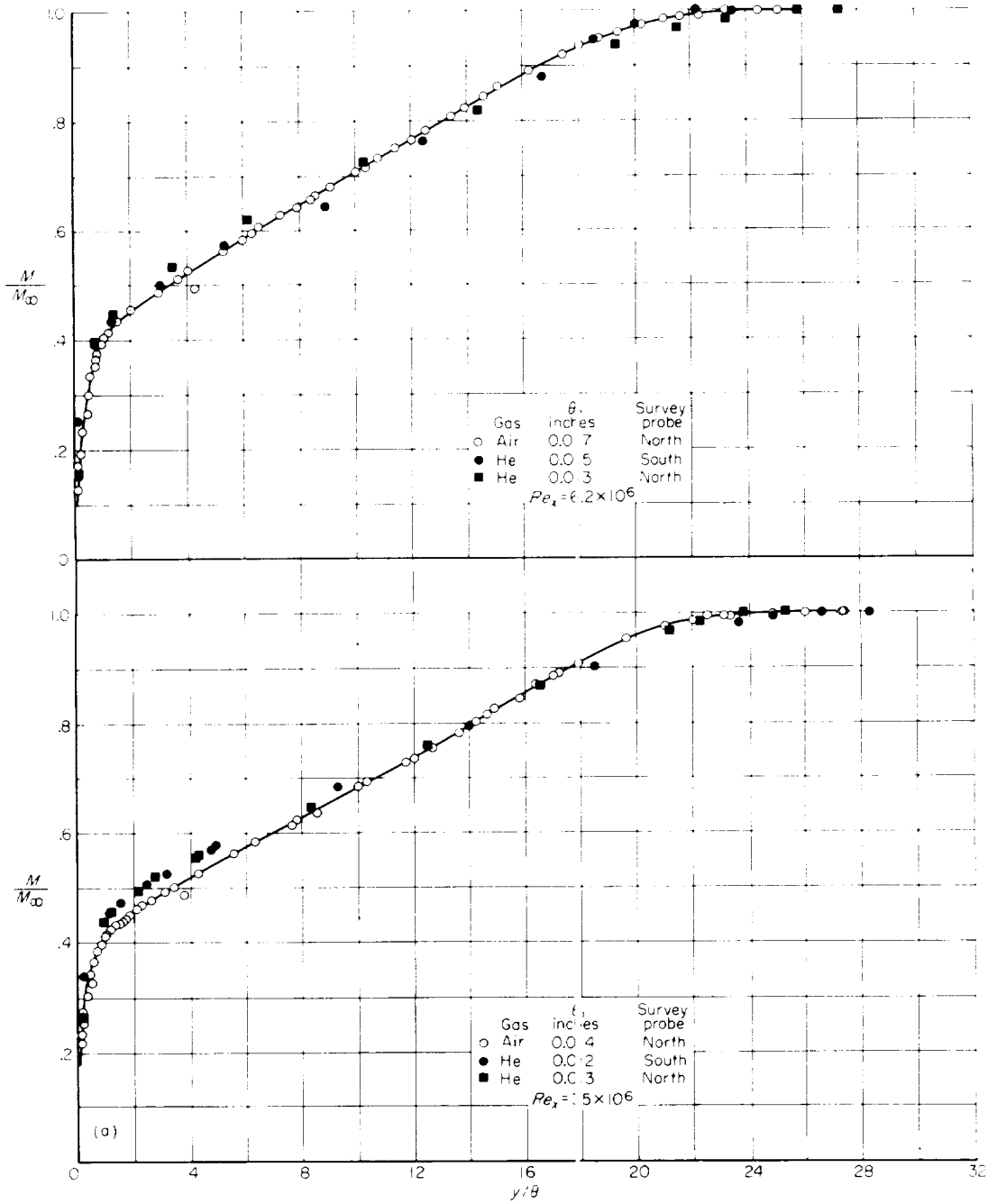

(a) $\frac{M}{M_\infty}$ vs. $\frac{y}{\theta}$

FIGURE 17. Equivalence of air and helium turbulent boundary-layer profiles; $M_a = 4.2$.

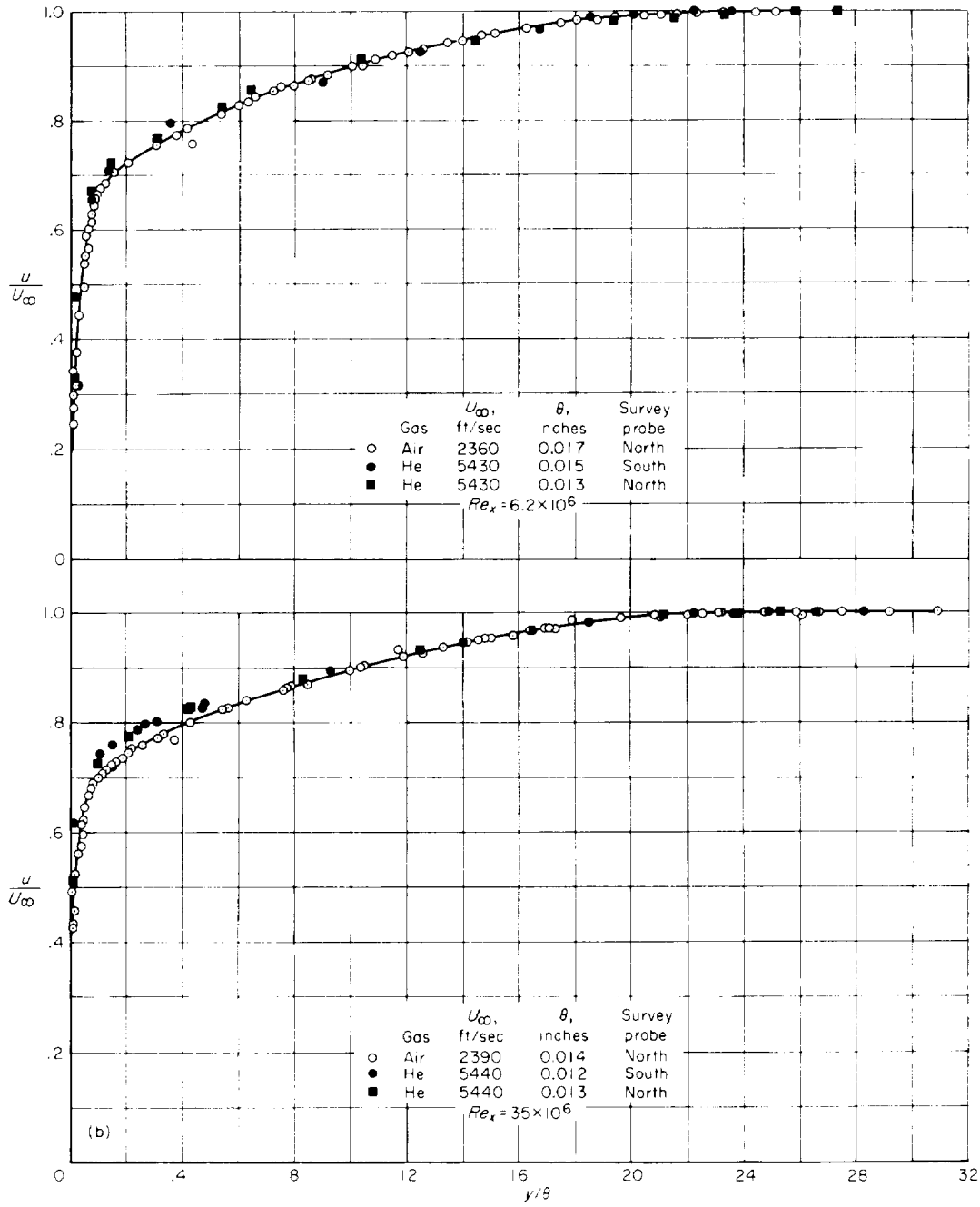

(b) $\frac{u}{U_\infty}$ vs. $\frac{y}{\theta}$

FIGURE 17 –Continued.

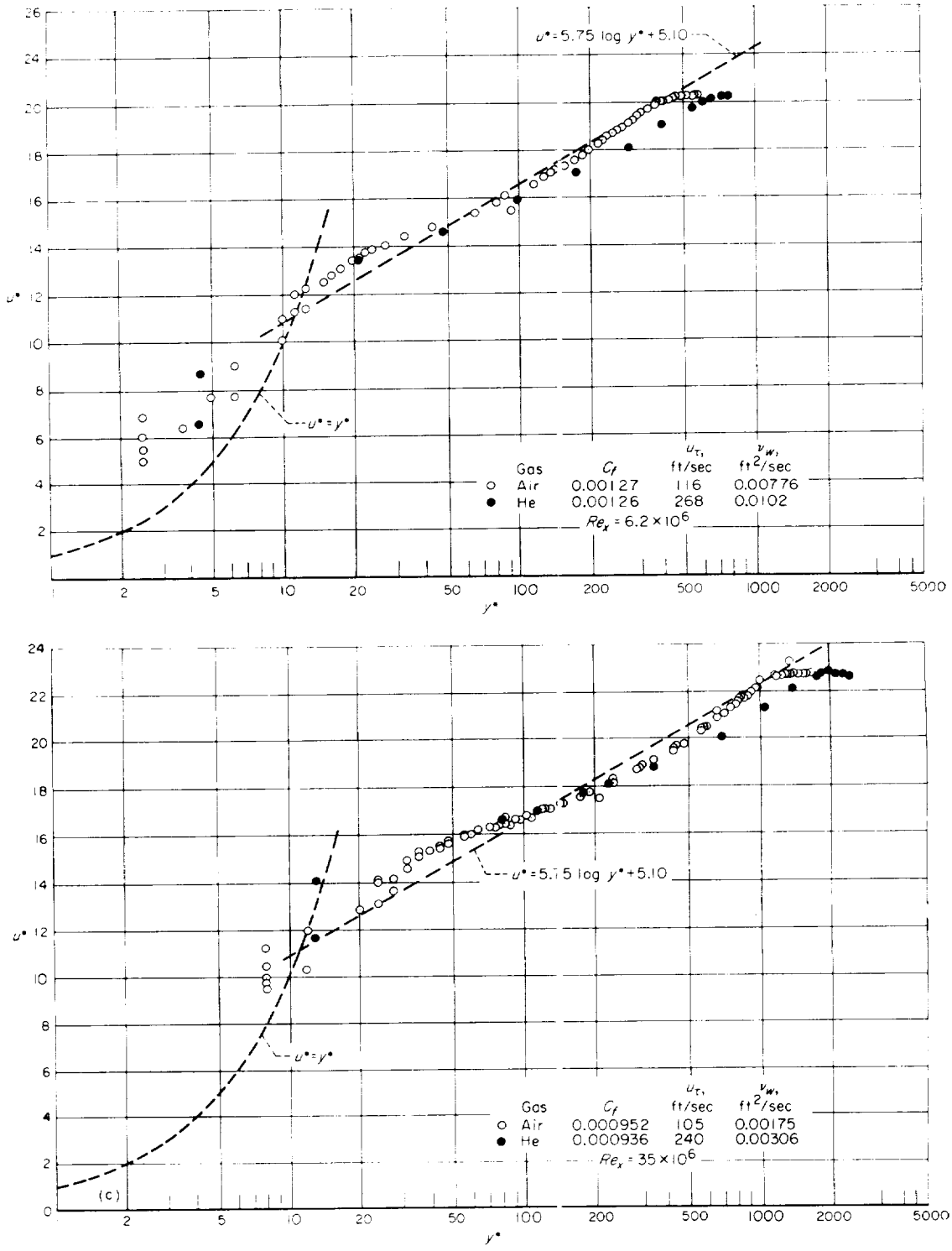

(c) u^* vs. y^*

FIGURE 17—Concluded

origin, Re_x (with the other parameters held fixed). However, it is also of interest to observe the skin-friction data as it was obtained, with the Reynolds number length measured from a fixed point in the wind tunnel. These data are presented in figure 18 with the Reynolds number, Re_L, measured from the nozzle throat. (For consistency, subsonic Reynolds numbers were also measured from this same location for this figure.) Figure 18 shows the type of data obtained when the Reynolds number is not corrected for the location of the virtual origin, and it also shows the transition characteristics of the wind tunnel. The solid data points to the left of the peaks show transition in process but not completed; these points do not represent turbulent data. The solid points to the right of the peaks represent turbulent data, but with transition less than 8 inches ahead of the element center. The solid points are not considered representative of fully turbulent flows and are not shown on any other figures. As mentioned previously the flagged points represent turbulent data with transition between 8 and 14 inches ahead of the element center ($Re_L - Re_x > 0.40\ Re_L$) and are of lesser accuracy than the high Reynolds number data with transition farther upstream (unflagged points); these points are also flagged on all subsequent figures. The curves of figure 18 are not considered to represent universal relationships between local skin friction and Reynolds number since the flow was not turbulent over the entire length on which Reynolds number was based.

With the Reynolds number measured from the virtual origin of the turbulent boundary layer, the relationship between C_f and Re_x is the universal one. The data are presented in this form in figure 19. It is seen that the flagged points tend to become somewhat erratic at the lowest Reynolds numbers (which are difficult to determine accurately as previously discussed). It is thought that

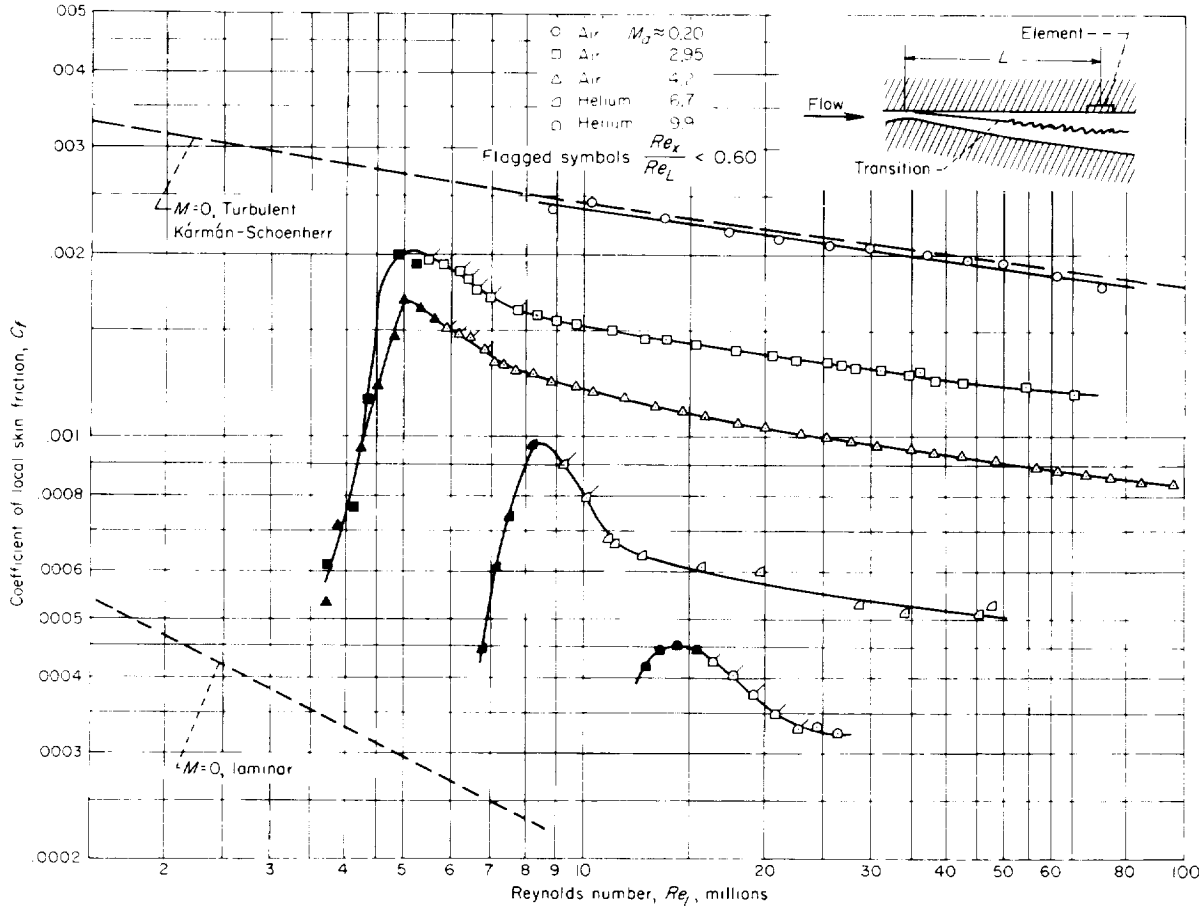

FIGURE 18.—Variation of flat-plate turbulent skin friction with Reynolds number based on length from nozzle throat.

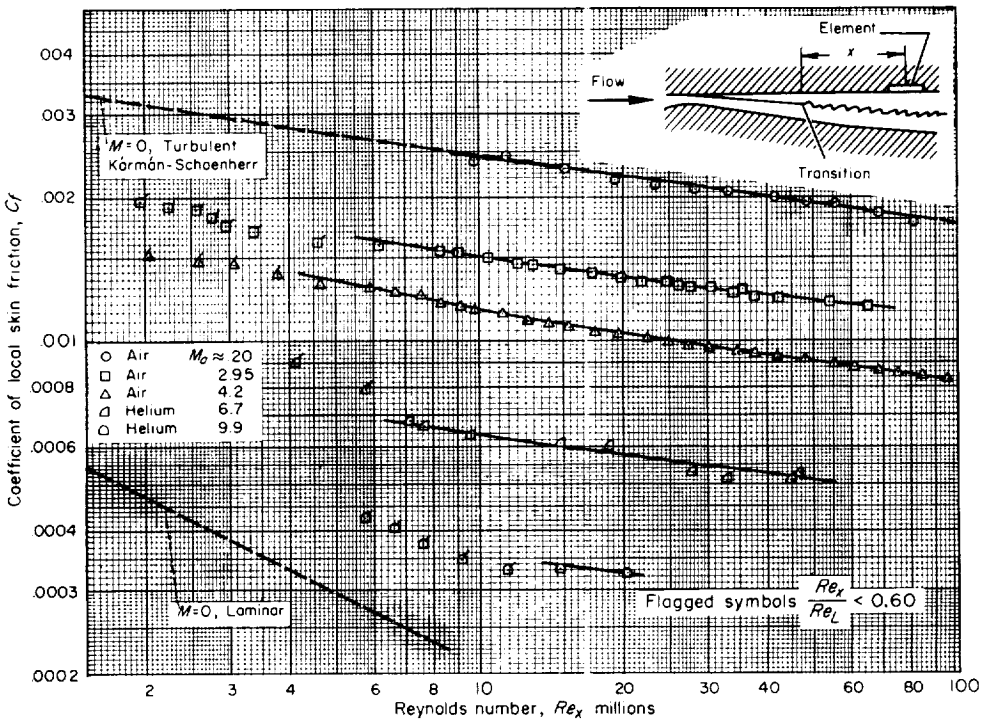

FIGURE 19.—Variation of flat-plate turbulent skin friction with Reynolds number based on length from virtual origin.

the unflagged points provide accurate values of the coefficient of local skin friction for the Mach numbers and Reynolds numbers at which the data were obtained. The subsonic data are in close agreement with the Kármán-Schoenherr curve for incompressible flow which has been included here for comparison purposes.

The present data have been compared with that taken by other investigators. The ranges of Mach numbers and Reynolds numbers over which comparison was possible are shown in figure 20 in which faired curves representing the present data are compared with faired curves representing data taken by Schultz-Grunow (ref. 30), Smith and Walker (ref. 4), and Coles (ref. 29). It is noted that the comparison is reasonably good in all cases. At $M_a=0.20$, the present data and the subsonic data of Schultz-Grunow and Smith and Walker fall on almost the same curve.

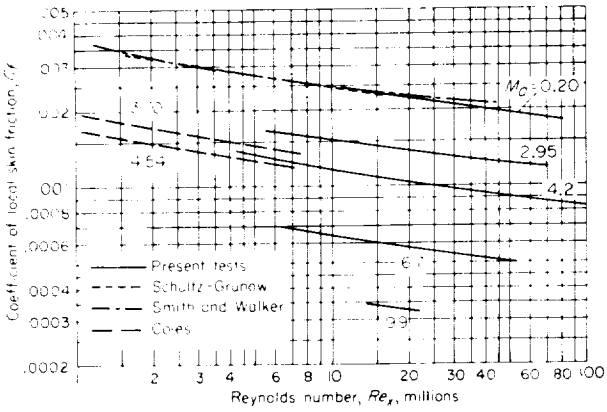

FIGURE 20.—Comparison of direct force measurements of turbulent skin friction.

In perhaps the most convenient form, the present data are summarized in figure 21 showing the ratio of the local skin-friction coefficient to the incompressible local skin-friction coefficient (Kármán-Schoenherr) at the same Reynolds number, C_f/C_{f_i}, as a function of Reynolds number, Re_x. Comparison of the levels of the curves shows the large effect of Mach number on C_f/C_{f_i}. Any Reynolds number effect on C_f/C_{f_i} for a given Mach number can be seen to be small. In examining the unflagged points, it is difficult to discern any strong Reynolds number trend within the scatter of the experimental data. It appears that for all practical purposes, C_f/C_{f_i} can be regarded as independent of Reynolds number. This is the same result as that previously obtained on bodies of revolution by Chapman and Kester (ref. 18) over a more limited range of test conditions.

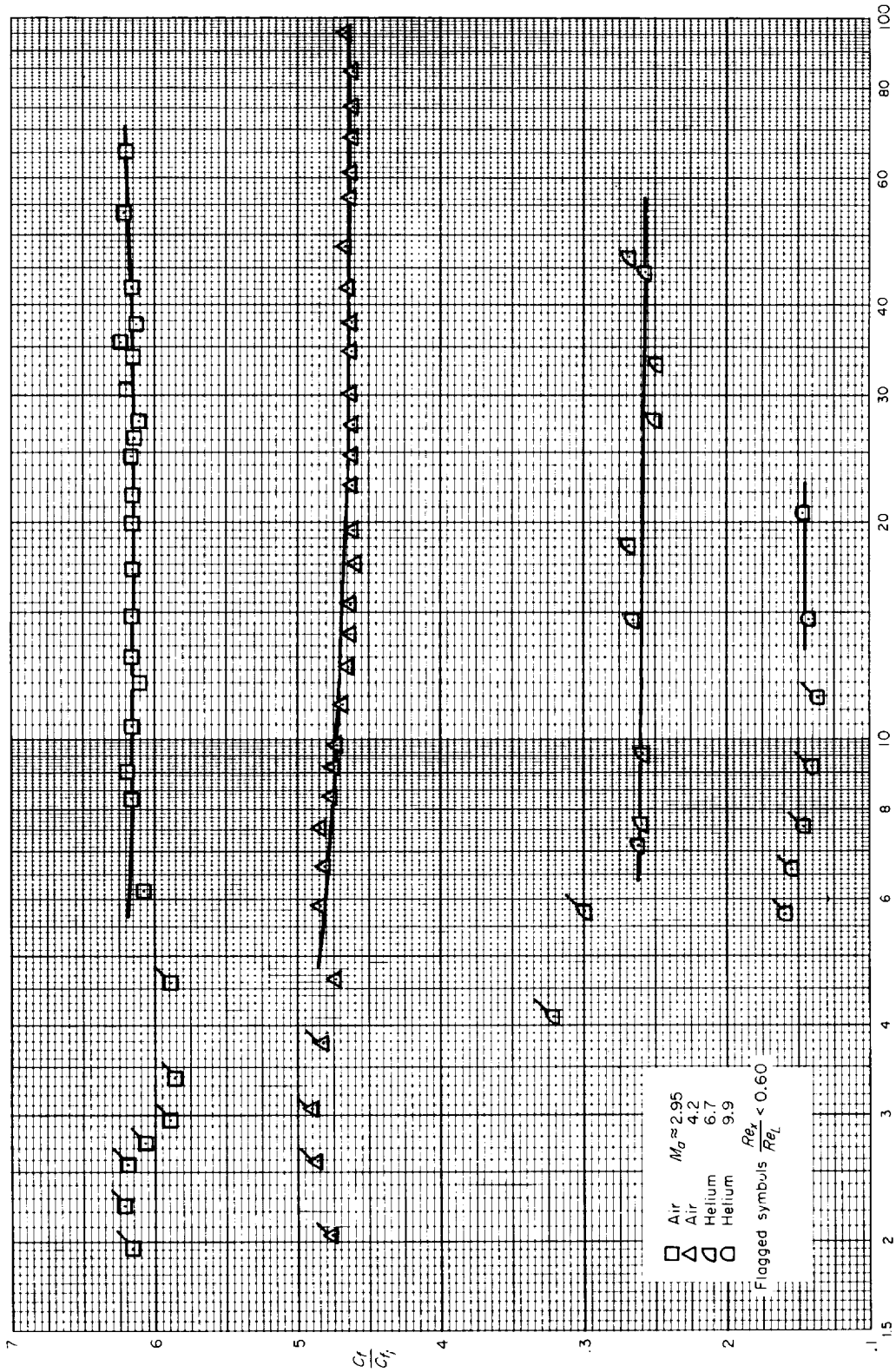

FIGURE 21.—Effect of Reynolds number on C_f/C_{f_i}.

COMPARISON OF EXPERIMENTAL RESULTS WITH METHODS OF CALCULATION

The experimental values obtained for the coefficient of local skin friction were compared with the results of four methods of calculating local skin friction in the compressible turbulent boundary layer: the T' method (ref. 19), the method of Walz (ref. 31), the Van Driest method using the Prandtl mixing length (ref. 21), and the Van Driest method using the Von Kármán mixing length (ref. 32). The four methods are not necessarily considered "best" by the authors, but were selected as being representative examples from the large number of methods proposed for calculating skin friction in the compressible turbulent boundary layer. The comparisons are shown in figure 22. In calculating the ordinate, C_f/C_{f_i}, the C_{f_i} value in all cases was taken as the Kármán-Schoenherr value.

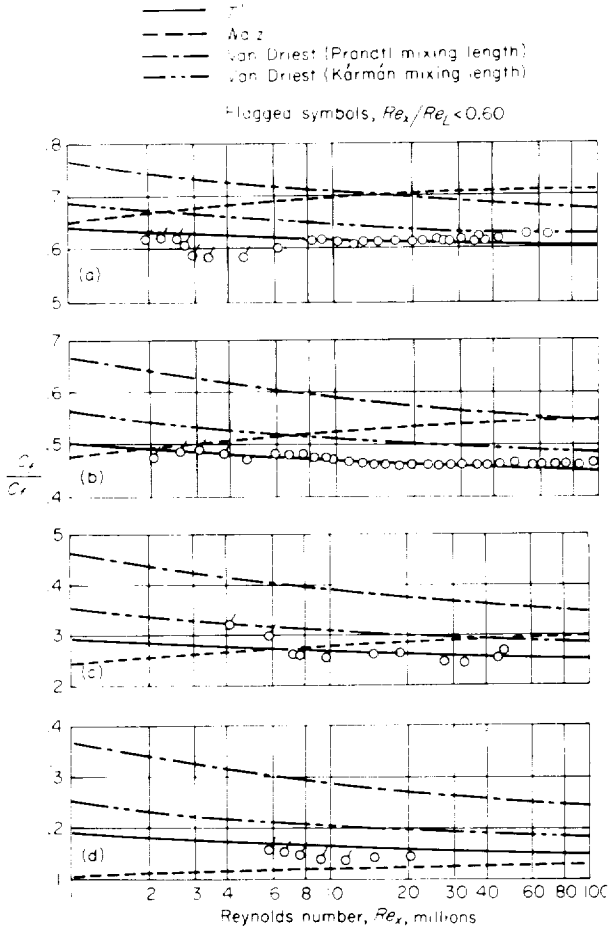

(a) $M_a = 2.95$
(b) $M_a = 4.2$
(c) $M_a = 6.7$
(d) $M_a = 9.9$

FIGURE 22.—Calculated C_f/C_{f_i} compared with experimental C_f/C_{f_i}.

It is noted that of the four methods the T' (intermediate enthalpy) method appears to give the best fit to the experimental data. The T' method uses a means reference temperature to evaluate the physical properties of the gas. It was originally used by Rubesin and Johnson (ref. 33) for laminar flows and was adapted to turbulent flows by Eckert, Sommer and Short, and others. The constants used in the calculations are those determined by Sommer and Short (ref. 19). (Constants obtained by other investigators do not change the results much.) It is seen that the experimental data and the T' calculations agree reasonably well although the trends with Reynolds number are not in complete agreement. The results of the T' calculations are somewhat affected by the viscosity temperature relationship used for the gas in the boundary layer. This means that the results for air and helium will differ slightly. The results for air are also affected by the temperature levels of the air (T_t or T_∞) since the dimensionless viscosity temperature relationship for air depends on the temperature level used. The T' curves in figure 22 were calculated for air at wind-tunnel temperatures to compare with data taken at equivalent air Mach numbers of 2.95 and 4.2; the T' curves were calculated for helium to compare with data taken at equivalent air Mach numbers of 6.7 and 9.9. These calculations correspond to the actual running conditions in the boundary-layer channel. The effects on the T' results of different temperature levels (with air) and of changing from air to helium are shown in figure 23. On a percentage (but not absolute) basis, the spread of these C_f/C_{f_i} curves increases with increase in Mach number.

Calculations of the coefficient of the local skin friction by the method of Walz are also shown in figure 22. This is a semiempirical integral method that makes use of results obtained from calculations of incompressible flows. It is seen in the figure that some values of C_f/C_{f_i} calculated by this method are higher and some are lower than the experimental points, but, in all cases, they increase with increasing Reynolds number at a given Mach number. This trend is not strong, but the trend of the curves does not fit the experimental data closely. By a visual extrapola-

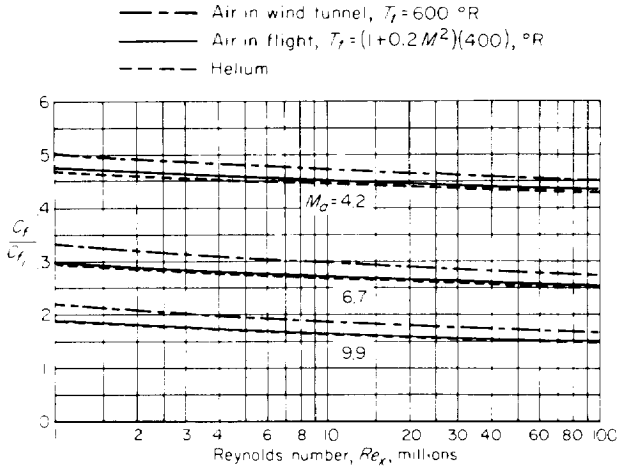

FIGURE 23.—Effect of temperature levels and gas properties on skin friction calculated by the T' method.

tion, it can be seen that these calculated curves will cross the curves of experimental data at some Reynolds number.

As seen in figure 22, the values of C_f/C_{f_i} calculated by the Van Driest method with Prandtl mixing length run consistently higher than the experimental data. Also the C_f/C_{f_i} values fall off fairly rapidly with increasing Reynolds number, whereas the experimental data do not indicate this effect. Values calculated by the Van Driest method with Von Kármán mixing length are considerably closer to the experimental data (although still a little high), and the slopes of the curves correspond more closely to the trend of the data.

SUBSONIC DATA AND POSSIBLE ROUGHNESS EFFECTS

Subsonic data were taken principally to determine the accuracy and validity of the experimental techniques used, since these data could be compared with the well-known properties of the low-speed turbulent boundary layer. Specifically, it was desired to find out whether the supersonic data could possibly contain any roughness effects. It has been shown that high Mach number boundary layers are less sensitive to roughness than are subsonic boundary layers (ref. 34). The subsonic and supersonic data were taken with the same top plate and skin-friction element, so that the roughness, if any, was invariant. Any roughness effects, then, would appear most strongly in the subsonic data. As is well known, when appreciable roughness exists, the subsonic skin-friction curve should, with increasing Reynolds number for a fixed length, diverge upward from the curve for a smooth surface and eventually become horizontal. As seen in figure 19, the subsonic data exhibit no such roughness effects. It is therefore believed that the supersonic data are free of roughness effects.

BOUNDARY-LAYER PROFILES

Although the main purpose of this research was to obtain and report skin-friction measurements, it was clearly of interest also to secure some boundary-layer profiles which would at least provide a qualitative "look" at the boundary layers being studied. Typical profiles are shown in figures 24, 25, and 26, the coordinates in figure 24 being M/M_∞ against y/θ, the coordinates in figure 25 being u/U_∞ against y/θ for the same profiles, while in figure 26 the same profiles again were plotted with u^* against y^*.

The M/M_∞ against y/θ plots in figure 24 represent data directly reduced from pitot traverses. It is seen that all of the M/M_∞ profiles are somewhat similar in shape; however, some variation in shape with change in Mach number can be seen. A decrease in θ/δ with increase in Mach number is readily recognized. Also it is seen that M/M_∞ at the edge of the sublayer decreases with an increase in Mach number. In physical dimensions the sublayer becomes thicker with an increase in Mach number although this is not readily seen from the normalized coordinates used in the plots. No corrections were made to the pitot readings to account for the fluctuating (turbulent) component of velocity since it was felt that these corrections would be small and would be less than the experimental scatter of the data. If these corrections had been made, the Mach numbers near the wall would have been reduced by a few percent since the pitot probe senses values higher than the time mean in turbulent flow. Also, as discussed below, it is believed that the largest error by far, is that of the distortion of the boundary layer due due to the presence of the probe. As observed previously in discussion of figure 17, a transverse variation in the value of θ of approximately 11 percent can also be seen in figure 24(a) which shows surveys taken on either side of the skin-friction element. The profiles again fall together when plotted on a y/θ basis.

The profiles in figure 25 convey essentially the

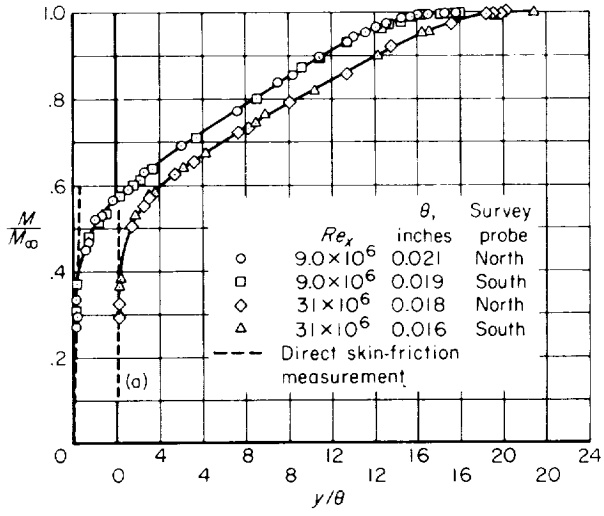

(a) $M_a=2.95$; air

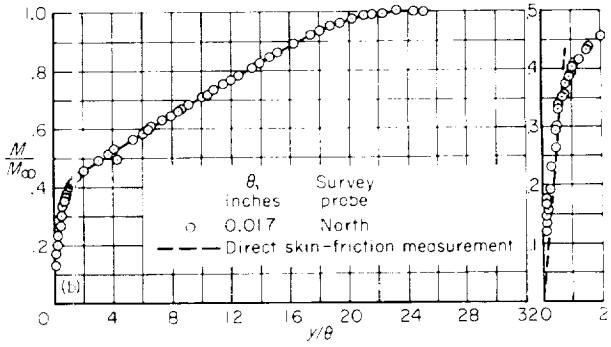

(b) $M_a=4.2$; air; $Re_x=6.2\times10^6$

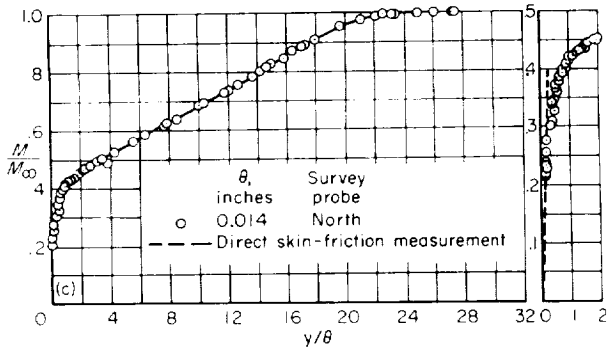

(c) $M_a=4.2$; air; $Re_x=35\times10^6$

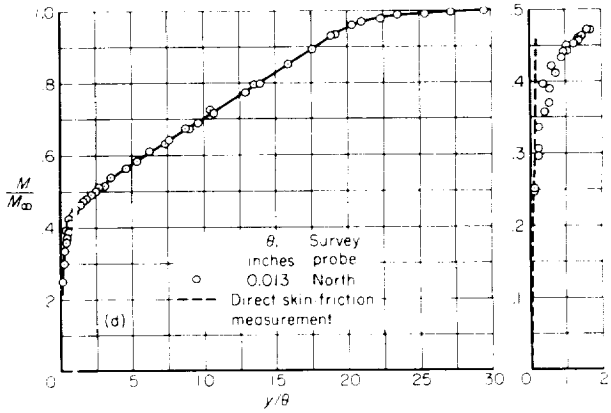

(d) $M_a=4.2$; air; $Re_x=69\times10^6$

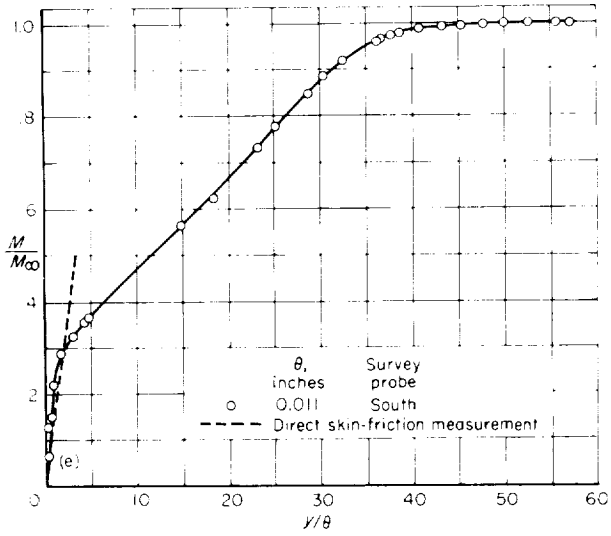

(e) $M_a=6.7$; helium; $Re_x=7.2\times10^6$

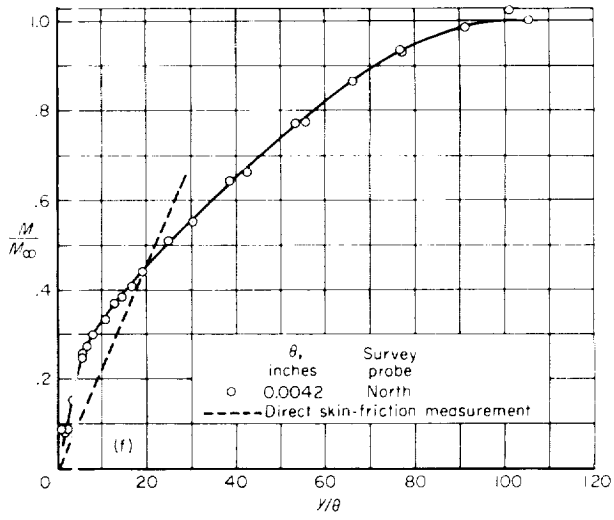

(f) $M_a=9.9$; helium; $Re_x=7.3\times10^6$ (C_f flagged)

FIGURE 24.—Turbulent boundary-layer Mach number profiles.

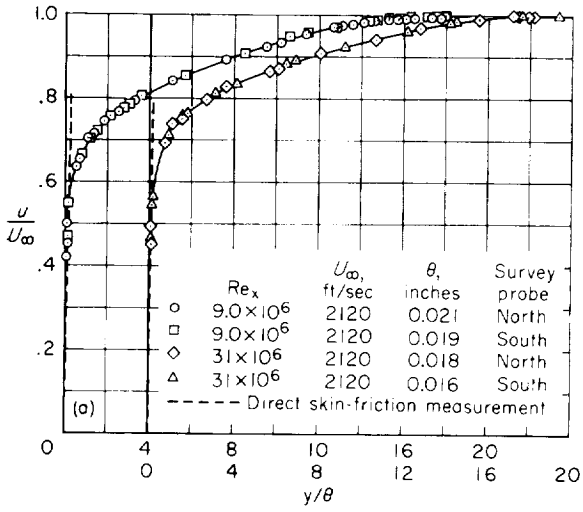

(a) $M_a=2.95$; air

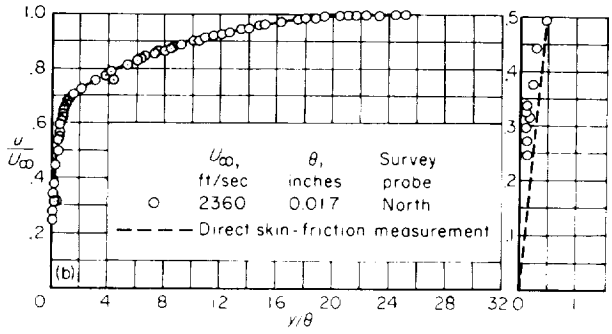

(b) $M_a=4.2$; air; $Re_x=6.2\times10^6$

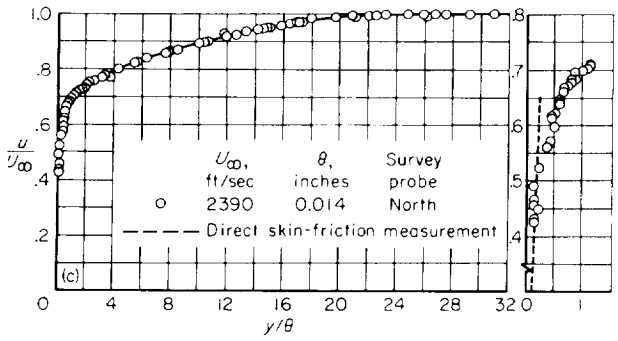

(c) $M_a=4.2$; air; $Re_x=35\times10^6$

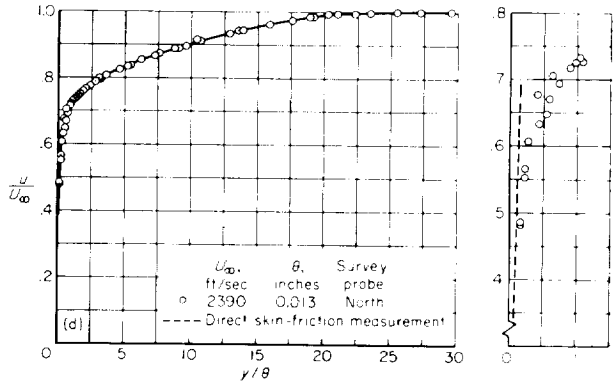

(d) $M_a=4.2$; air; $Re_x=69\times10^6$

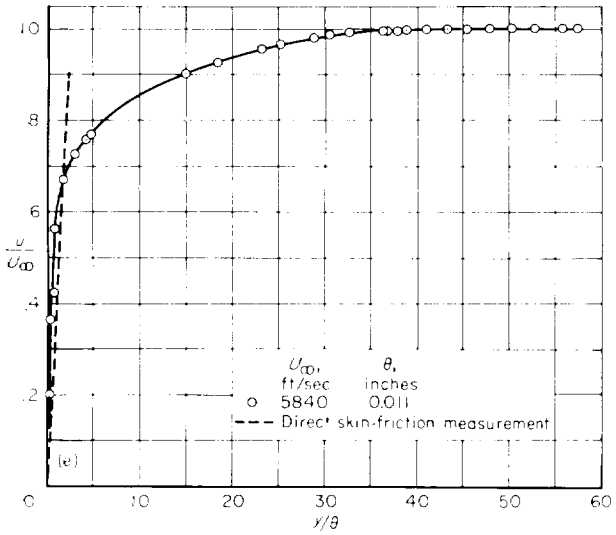

(e) $M_a=6.7$; helium; $Re_x=7.2\times10^6$

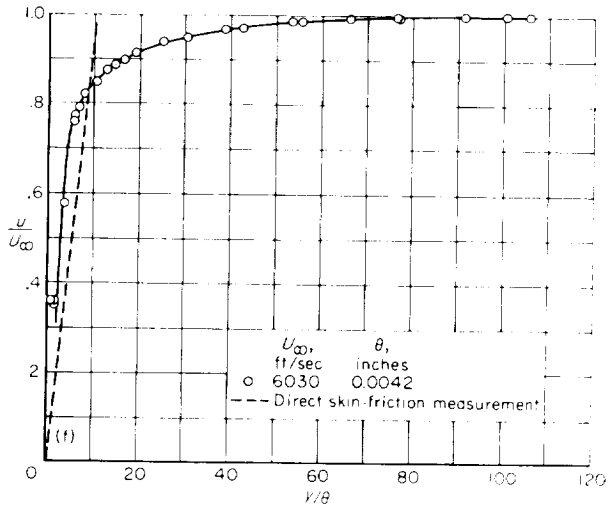

(f) $M_a=9.9$; helium; $Re_x=7.3\times10^6$ (C_f flagged)

FIGURE 25.—Turbulent boundary-layer velocity profiles.

same information, in somewhat different form, as the profiles in figure 24. The velocity, u, was calculated from the pitot data by assuming a constant total temperature (settling chamber temperature) through the boundary layer. This assumption, slightly in error, gives calculated velocities as much as approximately 5 percent too high near the wall (assuming the pitot Mach number is correct). With profiles plotted on a dimensionless velocity basis, the points are more spread out near the wall (in the sublayer) than when plotted on an M/M_∞ basis, as most of the velocity gradient occurs in the wall portion of the boundary layer.

Also shown on each profile in figures 24 and 25 is a straight line from the origin with slope determined by the directly measured coefficient of local skin friction. (Where profiles from north and south probes are superposed, average values of θ were used in calculating the slope of the straight line.) It is noted that with increasing Mach numbers there is an increasing discrepancy between the slope deduced from skin-friction measurements and the apparent slope of the measured profiles. This difference is presumably not due to any transverse nonuniformities in the flow as this difference was sensed by probes on either side of the skin-friction element. It is believed that the direct measurements of skin friction provide the more accurate determination and that the observed difference is largely due to the distortion of the sublayer by the presence of the probe in the sublayer. This effect may be three-dimensional, with the slower streamlines near the wall being displaced sidewards and the faster streamlines (located away from the wall) being displaced toward the wall. This could account for a probe near the wall sensing higher velocities than would normally be expected. Similar distortions in turbulent incompressible flows have been observed by a number of investigators. G. I. Taylor reported on experiments with a Stanton tube showing a Reynolds number effect on the distortion (ref. 35). Von Doenhoff showed a similar Reynolds number effect with a total pressure tube in contact with a surface (ref. 36). There are very few data for probes located away from the wall. Young and Maas (ref. 37) made pitot measurements in a wake, but their conclusion that the streamline displacement is approximately one-fourth of the probe diameter seems too small for the turbulent boundary layer. As pointed out by Von Doenhoff, the Young and Maas displacement is not large enough to be consistent with values measured at the wall (and it should also have a Reynolds number dependence as determined from measurements at the wall).

The apparent distortion of the boundary layer near the wall observed by the authors is of the same order of magnitude as that reported by Taylor and Von Doenhoff. In noting the disagreement between the measured profile slope near the wall and the slope deduced from the skin friction, it is felt that caution should be exercised in placing a high degree of reliance on pitot data in compressible turbulent flows near a wall.

In figure 26 the same data are plotted showing $u^*=u/u_\tau$ against $y^*=yu_\tau/\nu_w$. The north and south probes are not distinguished in this figure, and in the cases where two profiles were obtained simultaneously, average values of u and y were used in calculating u^* and y^*. Also, because of overcrowding, points near the outer edge of the boundary layer were thinned out where necessary for this figure. For purposes of comparison, the curves, $u^*=y^*$, and $u^*=5.75\ \log_{10}y^*+5.10$ are shown in figure 26. The constants in the latter equation (for incompressible flows) are obtained from reference 38. In figure 26(g) are plotted one profile for each Mach number, all at approximately the same Reynolds number. It is seen that all of these profiles have approximately the same shape. With the small amount of data obtained in the sublayer and at the edge of the sublayer, it does not appear to be possible to distinguish a definite trend with Mach number of the variation of u^* and y^* at the edge of the sublayer.

If the profiles in figures 24 and 25 were to be arbitrarily shifted to correspond to the measured skin-friction values, a similar correction would be made in the u^* vs. y^* profiles in figure 26. This would correspond to the so-called Nikuradse shift and would be of approximately the same order of magnitude (ref. 39). As reported in reference 39 Nikuradse arbitrarily shifted his u^* vs. y^* profiles outward by a constant amount so that the points nearest the wall would be consistent with the skin friction. In the absence of data giving accurate values of probe-induced distortion throughout the boundary layer, it would appear that a shift of the entire profile is not warranted. However, it should be kept in mind that the portion of the

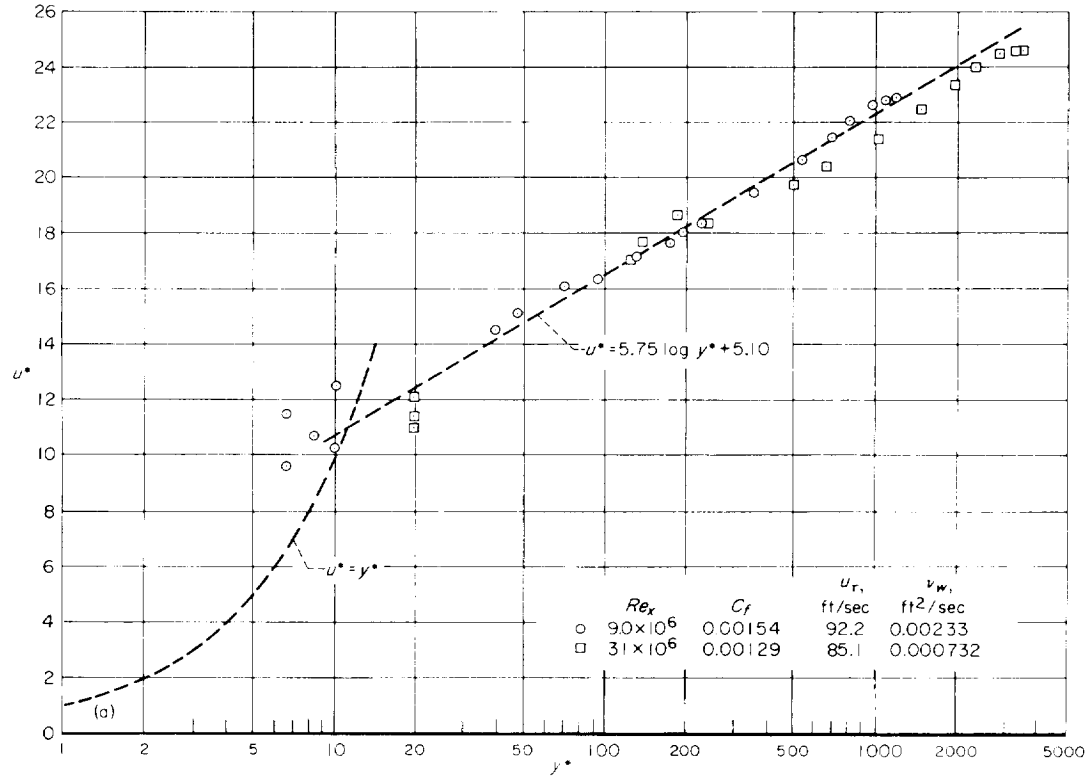

(a) $M_a = 2.95$; air

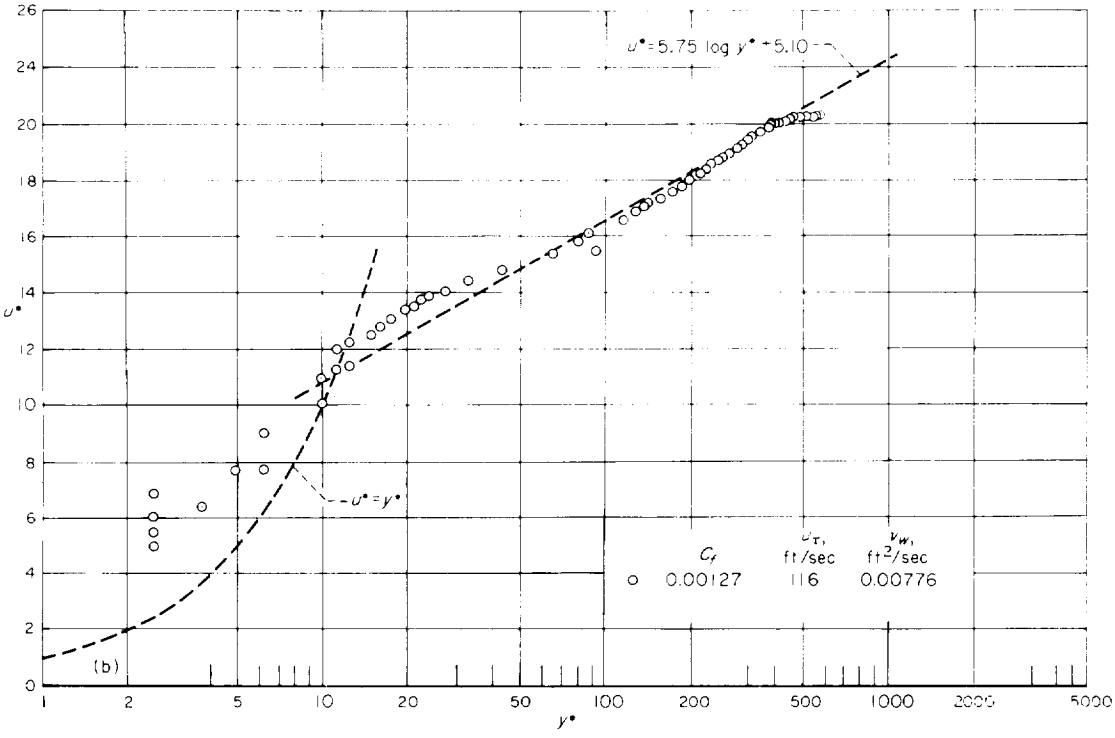

(b) $M_a = 4.2$; air; $Re_x = 6.2 \times 10^6$

FIGURE 26.—Turbulent boundary-layer profiles, u^* vs. y^*.

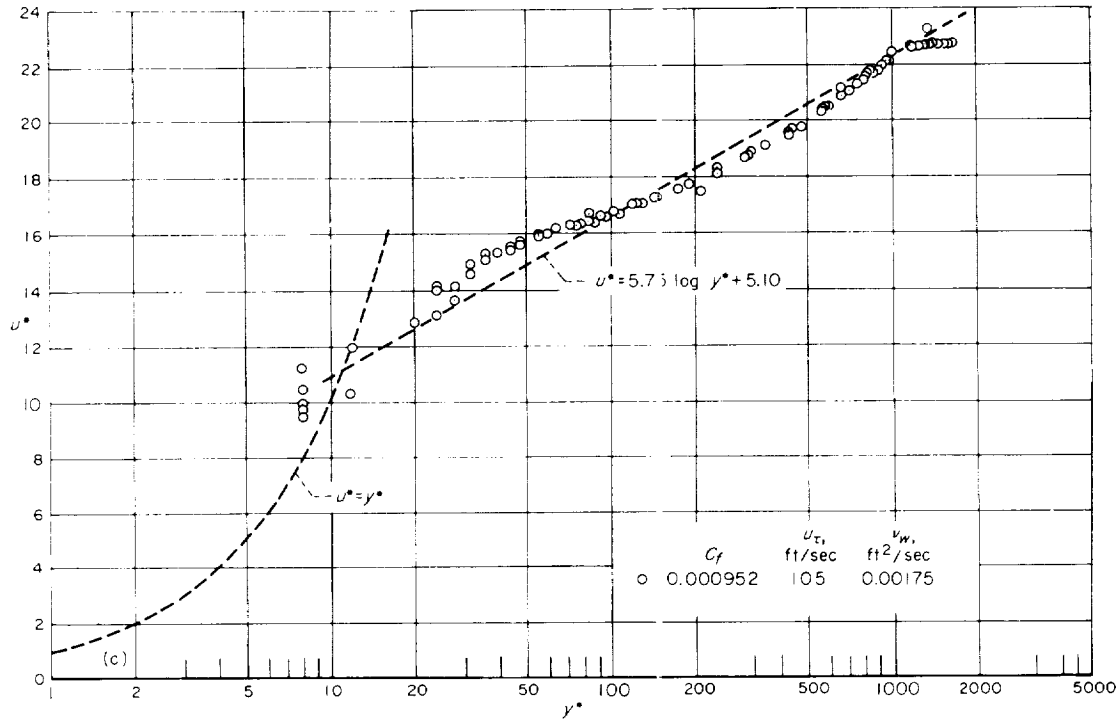

(c) $M_a = 4.2$; air; $Re_x = 35 \times 10^6$

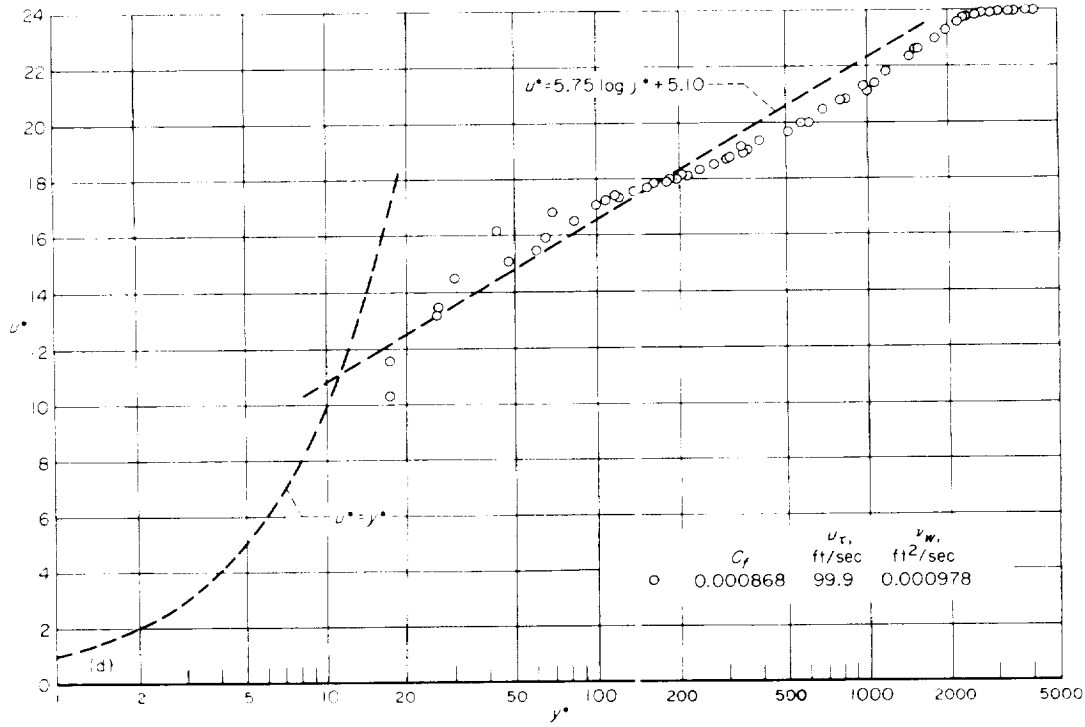

(d) $M_a = 4.2$; air; $Re_x = 69 \times 10^6$

FIGURE 26.—Continued

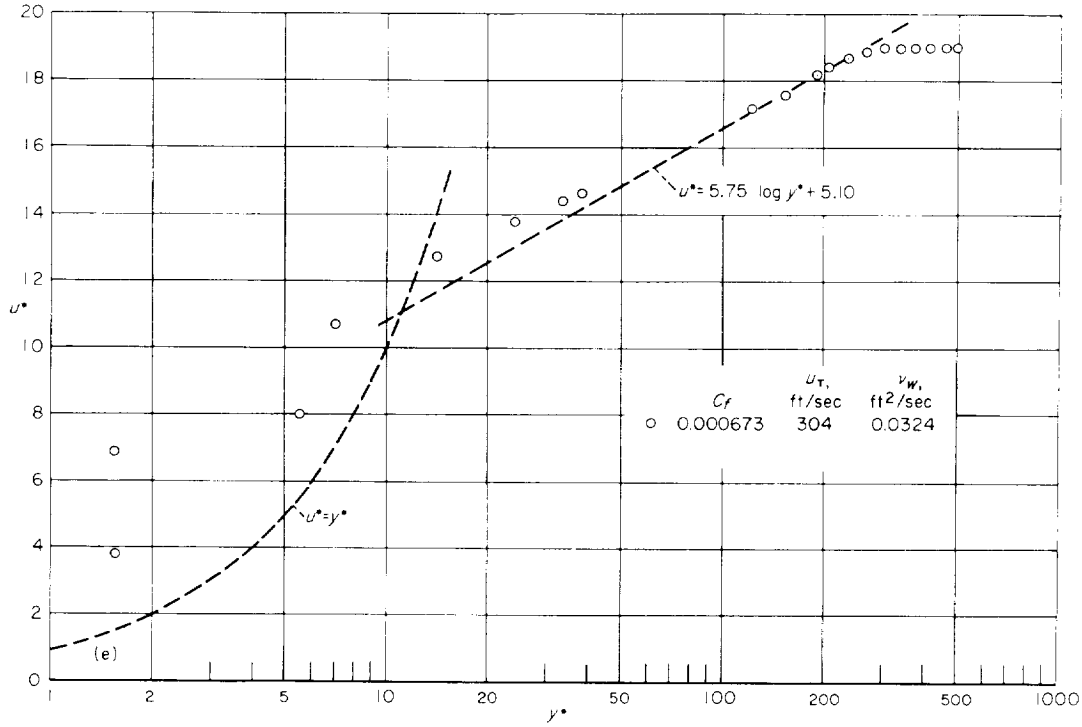

(e) $M_a = 6.7$; helium; $Re_x = 7.2 \times 10^6$

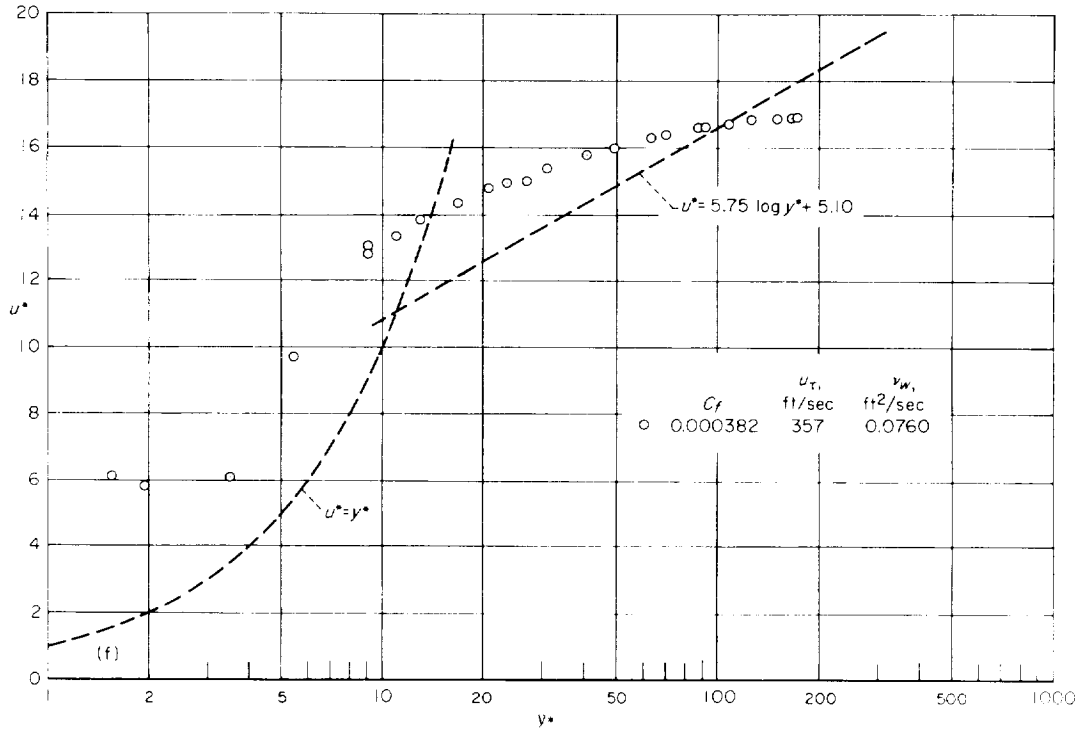

(f) $M_a = 9.9$; helium; $Re_x = 7.3 \times 10^6$ (C_f flagged)

FIGURE 26.—Continued

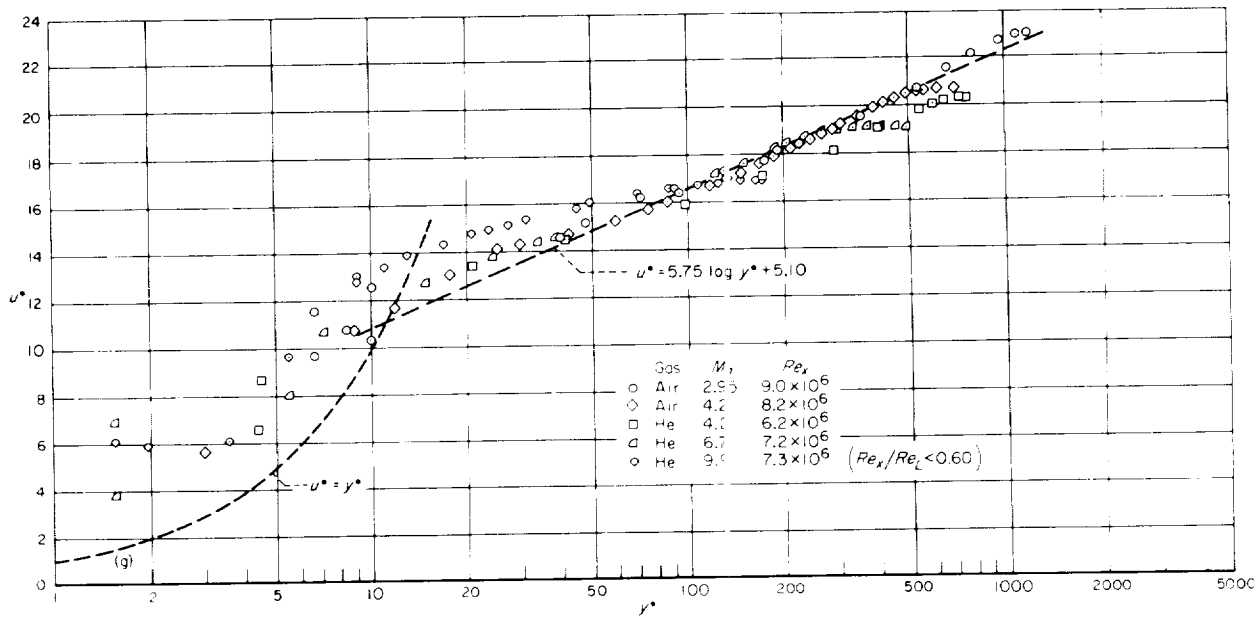

(g) Mach numbers indicated.

FIGURE 26.—Concluded

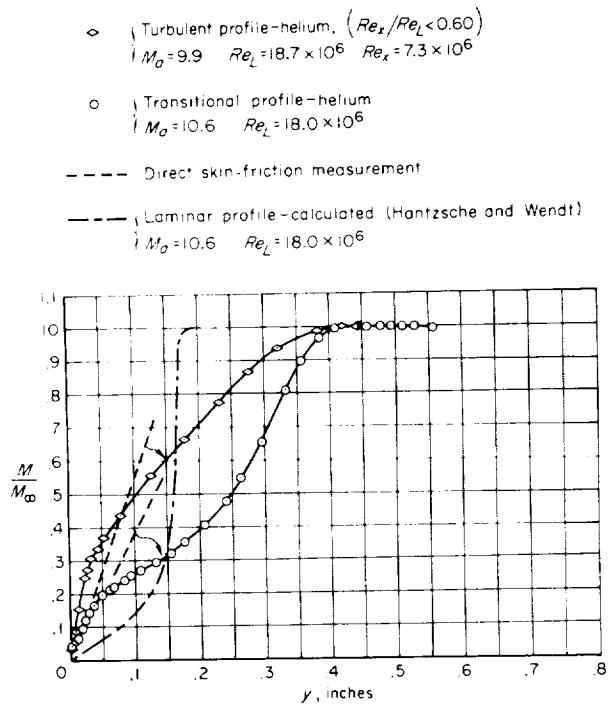

FIGURE 27.—Comparison of laminar, turbulent, and transitional profiles.

profile near the wall becomes somewhat distorted by the presence of a probe, and the data points near the wall are probably not reliable while those away from the wall probably are. Shifting the entire profile by a constant amount would scarcely be noticed for points far removed from the wall, but it would, of course, affect the points near the wall.

As a matter of interest, figure 27 has been included to show a comparison between a turbulent profile, a transitional profile, and a calculated laminar profile (ref. 40), all at approximately the same Reynolds number from the nozzle throat, Re_L, and all at equivalent air Mach numbers near 10. It is of interest to note that the slope of the straight line deduced from skin-friction measurements checks reasonably well with the wall slope of the transitional profile. As has been pointed out, these slopes did not check each other with the high Mach number turbulent profiles that were obtained, including the one shown in figure 27. It would appear that the probe produces less distortion near the wall for transitional boundary-layer profiles than for turbulent profiles. The explanation for this is not known.

CONCLUSIONS

Skin friction was measured in constant-pressure, adiabatic, turbulent boundary layers up to a maximum Reynolds number of 100×10^6 (at $M_a=4.2$) and up to a maximum equivalent air

Mach number of 9.9. Air and helium were used as test media. From the data obtained, the following conclusions have been drawn:

1. It is possible to set up equivalent, constant-pressure, turbulent boundary layers using different gases as test media. Measurements of skin friction taken with helium agree closely with those taken with air when $(\gamma-1)M_\infty^2$ is the same for the two gases and wall conditions are adiabatic.

2. The variation of the coefficient of local skin friction as calculated by the T' method agrees particularly well, while the Van Driest method with Von Kármán mixing length agrees reasonably well with experimental data over the range of test conditions investigated.

3. The experimental data indicate that the ratio, C_f/C_{f_i}, is essentially independent of Reynolds number.

AMES RESEARCH CENTER
NATIONAL AERONAUTICS AND SPACE ADMINISTRATION
MOFFETT FIELD, CALIF., *June 20, 1960*

APPENDIX A

EXPERIMENTAL DETERMINATION OF TEMPERATURE RECOVERY FACTOR

Adiabatic wall conditions in the turbulent boundary layers were established experimentally without actually knowing the temperature recovery factor. However, it is of interest to calculate the recovery factors as follows:

$$\eta_r = \frac{T_{aw} - T_\infty}{T_t - T_\infty} \tag{A1}$$

In more convenient form:

$$\eta_r = \frac{\frac{T_{aw}}{T_t}\left(1 + \frac{\gamma - 1}{2} M_\infty^2\right) - 1}{\frac{\gamma - 1}{2} M_\infty^2} \tag{A2}$$

Experimentally, the adiabatic wall temperature, T_{aw}, was taken as the existing wall temperature prior to the run. The Mach number was known prior to the run from previous measurements with the given nozzle and test section geometry. The total temperature, T_t, was adjusted before the run by setting the desired temperature in the heat exchanger. In operation the heat exchanger held the T_t constant within several degrees until the heat capacity of the exchanger was used up, at which time the T_t fell off rapidly, and the run was then terminated. The adiabatic condition was determined by the constancy of the wall temperature during the run. A 2° F change in wall temperature during a run was considered allowable for adiabatic operation.

Values of T_t were initially preset by calculation from expected values of η_r. Adjustments of T_t for subsequent runs were based on experience, with constancy of wall temperature as the criterion. Recovery factors were then calculated from the acceptable values of T_t.

Recovery factors were 0.87 for air at M_a values of 2.95 and 4.2. For helium the recovery factors were 0.86, 0.87, and 0.88 for M_a values of 4.2, 6.7, and 9.9, respectively.

APPENDIX B

ELECTRICAL CIRCUITRY OF THE SKIN-FRICTION ELEMENT AND SERVO

The electrical circuitry of the skin-friction element and servo was designed and the equipment constructed under the supervision of William J. Kerwin of the Ames Research Center. The skin-friction element transducer consists of two variable inductors whose inductances are changed in opposite directions by the motion of a magnetic armature (magnetic return piece) on the disk (see figs. 8 and 9). The armature varies the size of a small air gap and thus changes the reluctance of the magnetic path.

Figure 10 shows the double balance a-c bridge and associated circuitry used. The relations necessary for balance are:

$$\frac{L_1}{L_2}=\frac{R_0+\alpha R}{R_0+(1-\alpha)R} \tag{B1}$$

$$\frac{r_1}{r_2}=\frac{R_0+\alpha R}{R_0+(1-\alpha)R} \tag{B2}$$

where

L_1 variable inductance of skin-friction element coil No. 1

L_2 variable inductance of skin-friction element coil No. 2

R_0 fixed resistances in the bridge

R total resistance of potentiometer No. 1 (constant)

α fractional part of R

r_1 total resistance (variable) in skin-friction element coil No. 1 (fixed) and partial resistance of potentiometer No. 2 (variable)

r_2 total resistance (variable) in skin-friction element coil No. 2 (fixed) and partial resistance of potentiometer No. 2 (variable)

Since the inductances are approximately inversely proportional to the air gap spacing, one can write:

$$L_1=\frac{K_1}{g_0+g} \tag{B3}$$

$$L_2=\frac{K_1}{g_0-g} \tag{B4}$$

where

g_0 gap spacing with the element disk in the neutral position

g variation in gap spacing from the neutral position

K_1 constant of proportionality

Equation (B1) then reduces to:

$$\frac{g_0-g}{g_0+g}=\frac{R_0+\alpha R}{R_0+(1-\alpha)R} \tag{B5}$$

Solving for α one obtains

$$\alpha=\frac{1}{2}-\left(\frac{R+2R_0}{2g_0R}\right)g \tag{B6}$$

$$\Delta\alpha=-K_2\Delta g \tag{B7}$$

where

$$K_2=\frac{R+2R_0}{2g_0R}$$

Thus the reading of a counter connected to potentiometer No. 1 is directly proportional to the change in the gap spacing in the skin-friction element.

The bridge balance is accomplished by an automatic dual balance servo. One servomotor is connected to potentiometer No. 1 and is driven so as to null the component of bridge output voltage in quadrature with the applied bridge voltage, this component being introduced primarily by inductive unbalance of the bridge (eq. (B1)). A second servomotor is connected to potentiometer No. 2 and is driven so as to null the component of bridge output voltage which is in phase with the applied bridge voltage, this component being introduced primarily by resistance unbalance of the bridge (eq. (B2)). A 3000 count dial connected to the shaft of potentiometer No. 1 indicates the displacement of the disk in the skin-friction element.

REFERENCES

1. Schoenberr, Karl E.: Resistance of Flat Surfaces Moving Through a Fluid. Soc. Nav. Arch. and Marine Eng. Trans., vol. 40, 1932, pp. 279–313.
2. Locke, F. W. S., Jr.: Recommended Definition of Turbulent Friction in Incompressible Fluids. Bur. Aero., Navy Dept., (Design) Res. Div., DR Rep. 1415, 1952.
3. Hughes, G.: Frictional Resistance of Smooth Plane Surfaces in Turbulent Flow—New Data and Survey of Existing Data. Trans. Inst. Nav. Arch., vol. 94, 1952, pp. 287–322.
4. Smith, Donald W., and Walker, John H.: Skin-Friction Measurements in Incompressible Flow. NACA TN 4231, 1958.
5. Wilson, Robert E.: Turbulent Boundary-Layer Characteristics at Supersonic Speeds—Theory and Experiment. Jour. Aero. Sci., vol. 17, no. 9, Sept. 1950, pp. 585–594.
6. Rubesin, Morris W., Maydew, Randall C., and Varga, Steven A.: An Analytical and Experimental Investigation of the Skin Friction of the Turbulent Boundary Layer on a Flat Plate at Supersonic Speeds. NACA TN 2305, 1951.
7. Dhawan, Satish: Direct Measurements of Skin Friction. NACA Rep. 1121, 1953 (Supersedes NACA TN 2567).
8. Coles, Donald: Direct Measurement of Supersonic Skin Friction. Jour. Aero. Sci., vol. 19, no. 10, Oct. 1952, p. 717.
9. Brinich, Paul F., and Diaconis, Nick S.: Boundary-Layer Development and Skin Friction at Mach Number 3.05. NACA TN 2742, 1952.
10. Bradfield, W. S., DeCoursin, D. G., and Blumer, C. B.: Characteristics of Laminar and Turbulent Boundary Layer at Supersonic Velocity. Univ. of Minn., Inst. of Tech. Res., Rep. 83, 1952.
11. Cope, W. F.: The Measurement of Skin Friction in a Turbulent Boundary Layer at a Mach Number of 2.5, Including the Effect of a Shock Wave. Proc. Roy. Soc., ser. A, vol. 215, no. 1120, Nov. 1952.
12. Weiler, J. E., and Hartwig, W. H.: The Direct Determination of Local Skin Friction Coefficient. Univ. of Texas Defense Res. Lab., CF 1747, (UT/DRL 295), Jan. 1952.
13. Spivack, H. M.: Experiments in the Turbulent Boundary Layer of a Supersonic Flow. North American Aviation, Inc., Rep. no. CM-615 (AL-1052), 1950.
14. Monaghan, R. J., and Johnson, J. E.: The Measurement of Heat Transfer and Skin Friction at Supersonic Speeds. Part II. Boundary Layer Measurements on a Flat Plate at $M=2.5$ and Zero Heat Transfer. British ARC. CP 64, (13,064), 1952.
15. Ladenburg, I. R., and Bershader, Daniel: Optical Studies of Boundary Layer Phenomena on a Flat Plate at Mach Number 2.35. Princeton Univ., Dept. of Phys., Dec. 1952.
16. Bloom, H. L.: Preliminary Survey of Boundary-Layer Development at a Nominal Mach Number of 5.5. NACA RM E52D03, 1952.
17. Hakkinen, Raimo J.: Measurements of Turbulent Skin Friction on a Flat Plate at Transonic Speeds. NACA TN 3486, 1955.
18. Chapman, Dean R., and Kester, Robert H.: Turbulent Boundary-Layer and Skin-Friction Measurements in Axial Flow Along Cylinders at Mach Numbers Between 0.5 and 3.6. NACA TN 3097, 1954.
19. Sommer, Simon C., and Short, Barbara J.: Free-Flight Measurements of Turbulent-Boundary-Layer Skin Friction in the Presence of Severe Aerodynamic Heating at Mach Numbers From 2.8 to 7.0. NACA TN 3391, 1955.
20. Lobb, Kenneth R., Winkler, Eva M., and Persh, Jerome: NOL Hypersonic Tunnel No. 4 Results VII: Experimental Investigation of Turbulent Boundary Layers in Hypersonic Flow. NAVORD Rep. 3880, 1955.
21. Van Driest, E. R.: Turbulent Boundary Layer in Compressible Fluids. Jour. Aero. Sci., vol. 18, no. 3, Mar. 1951, pp. 145–160, 216.
22. Crocco, Luigi: Lo Strato Limite Laminare Nei Gas. Monografie Scientifiche Di Aeronautica, Ministere dell Aeronautica No. 3, 1946. See also Maximum Velocity in Laminar Flow of Gases. Tech. Intelligence Trans. F-TS-5053-RE, AMC, Wright Field, 1946.
23. Anon.: Tables of Thermal Properties of Gases. National Bureau of Standards Circular 564, 1955.
24. Keesom, W. H.: Helium. Elsevier, Amsterdam-New York, 1942.
25. Akin, S. W.: The Thermodynamic Properties of Helium. Trans. A.S.M.E., vol. 72, no. 6, Aug. 1950, pp. 751–757.
26. Love, Eugene S., Henderson, Arthur Jr., and Bertram, Mitchel H.: Some Aspects of Air-Helium Simulation and Hypersonic Approximations. NASA TN D-49, 1959.
27. Ames Research Staff: Equations, Tables, and Charts for Compressible Flow. NACA Rep. 1135, 1953.
28. Anon.: The NBS–NACA Tables of Thermal Properties of Gases. Table 2.39 Dry Air, Coefficients of Viscosity. F. C. Morey, Compiler, National Bureau of Standards, 1950.
29. Coles, Donald: Measurements in the Boundary Layer on a Smooth Flat Plate in Supersonic Flow. Part III. Measurements in a Flat-Plate Boundary Layer at the Jet Propulsion Laboratory. CIT, Rep. 20–71, June 1953.
30. Schultz-Grunow, F.: New Frictional Resistance Law for Smooth Plates. NACA TM 986, 1941.
31. Walz, Alfred: Nouvelle Méthode Approchée de Calcul des Couches Limites Laminaire et Turbulente en Écoulement Compressible. Publications Scientifiques et Techniques du Ministère de l'Air, No. 309, 1956.

32. Van Driest, E. R.: The Turbulent Boundary Layer With Variable Prandtl Number. North American Aviation, Inc., Rep. AL–1914, April 2, 1954.
33. Rubesin, M. W., and Johnson, H. A.: A Critical Review of Skin-Friction and Heat-Transfer Solutions of the Laminar Boundary Layer of a Flat Plate. Trans. A.S.M.E., vol. 71, no. 4, May 1949.
34. Goddard, Frank E., Jr.: Effect of Uniformly Distributed Roughness on Turbulent Skin-Friction Drag at Supersonic Speeds. Jour. Aero/Space Sci., vol. 26, no. 1, Jan. 1959, pp. 1–15, 24.
35. Taylor, G. I.: Measurements With a Half-Pitot Tube. Proc. Roy. Soc. (London), ser. A, vol. 166, 1938, pp. 476–481.
36. Von Doenhoff, Albert E.: Investigation of the Boundary Layer About a Symmetrical Airfoil in a Wind Tunnel of Low Turbulence. NACA WR–L–507, 1940.
37. Young, A. D., and Maas, J. N.: The Behaviour of a Pitot Tube in a Transverse Total-Pressure Gradient. R. & M. No. 1770, British A.R.C., 1937.
38. Coles, Donald: Measurements in the Boundary Layer on a Smooth Flat Plate in Supersonic Flow. Part I. The Problem of the Turbulent Boundary Layer. Jet Propulsion Laboratory, CIT, Rep. 20–69, June 1953.
39. Miller, Benjamin: The Laminar-Film Hypothesis. Trans. A.S.M.E., vol. 71, no. 4, May 1949, pp. 357–367.
40. Hantzsche, W., and Wendt, H.: Integration of the Laminar Boundary Layer Over a Flat Plate With and Without Heat Transmission. Headquarters, Air Materiel Command, Wright-Patterson Air Force Base, Dayton, Ohio. Translation Rep. F–TS–2072–RE, April 1948.

U.S. GOVERNMENT PRINTING OFFICE: 1961